https://doi.org/10.5194/egusphere-2026-3449
Preprint. Discussion started: 25 June 2026


# QBO-induced anomalous transport in the Northern Hemisphere stratosphere: the exceptional 2018/2019 late boreal winter

Daniele Minganti[1], Simon Chabrillat[1], Sean Davis[4], Quentin Errera[1], Marc Op de beeck[1], Eric Ray[4], Sarah Vervalcke[1], Krzysztof Wargan[2,3], and Catherine Wespes[1,5]

[1]Royal Belgian Institute for Space Aeronomy (BIRA-IASB), Uccle, Belgium
[2]NASA Goddard Space Flight Center, Maryland, USA
[3]Science Systems and Applications Inc., Maryland, USA
[4]NOAA Chemical Sciences Laboratory, Boulder, Colorado, USA
[5]Spectroscopy, Quantum Chemistry and Atmospheric Remote Sensing (SQUARES), Université Libre de Bruxelles (ULB), Brussels, Belgium

**Correspondence:** Daniele Minganti (daniele.minganti@aeronomie.be)

**Abstract.** Large positive anomalies of nitrous oxide ($N_2O$) were observed in the northern hemisphere lower stratosphere in the late 2018/2019 boreal winter. Thanks to its long lifetime in the lower stratosphere, $N_2O$ is a robust tracer for stratospheric transport. This study investigates the magnitude, vertical structure, and dynamical origin of the late 2018/2019 boreal winter $N_2O$ anomaly using multiple chemical transport model simulations, chemical reanalyses, a specified-dynamics chemistry-climate model, and merged satellite observations. All datasets consistently show pronounced $N_2O$ positive anomalies in February 2019 in the northern mid-latitudes at 50 hPa. The $N_2O$ Transformed Eulerian Mean budget indicates that the $N_2O$ anomalies are primarily driven by enhanced meridional residual advection, which is in turn determined by enhanced planetary wave forcing. The extratropical effects of the quasi-biennial oscillation (QBO) determine these transport anomalies: the poleward QBO secondary circulation was unusually strong in the late 2018/2019 boreal winter, and a marked northward displacement of the zero wind line induced the enhanced planetary wave forcing. The combined strengthening of both the northward QBO secondary circulation and the planetary wave forcing led to unusually strong poleward advection in the northern lower stratosphere, which ultimately built up the $N_2O$ positive anomalies. These results indicate the value of long-lived stratospheric tracers such as $N_2O$ for diagnosing dynamically driven extreme events and for disentangling the contributions of different transport processes. We highlight the importance of the QBO teleconnections, particularly as a warming climate may change the frequency and intensity of extreme events thereby impacting these teleconnections.

## 1 Introduction

Nitrous oxide ($N_2O$) is the fourth most important greenhouse gas (Tuckett, 2019) and participates in the destruction of ozone in the stratosphere (Crutzen, 1970). $N_2O$ is continuously emitted in the troposphere, through natural processes such as nitrification in the oceans and freshwater, and microbial nitrification in soils, but also through anthropogenic processes such as agriculture and biomass burning (Tian et al., 2020; Costa et al., 2021). The $N_2O$ concentrations in the atmosphere have been constantly increasing with an estimated rate of increase of 2% per decade (Tian et al., 2020). The only significant atmospheric destruction

https://doi.org/10.5194/egusphere-2026-3449
Preprint. Discussion started: 25 June 2026


of $N_2O$ occurs in the tropical upper stratosphere through photodissociation (Seinfeld and Pandis, 2016). The atmospheric lifetime of $N_2O$ is approximately 120 years (Prather et al., 2015), even though a recent analysis has shown that the $N_2O$ lifetime has been decreasing at around 2% per decade (Prather et al., 2023). This very long lifetime makes $N_2O$ an excellent tracer for transport studies in the stratosphere (Brasseur and Solomon, 2005).

One of the most relevant transport mechanisms in the stratosphere is the Brewer-Dobson Circulation (BDC, Brewer, 1949; Dobson and Massey, 1956). The BDC consists in upward motion over the tropical latitudes (upwelling), poleward transport followed by downward motion (downwelling) over the extra-tropical latitudes (Plumb, 2002). For the transport of tracers, the BDC is often divided into an advective component (the residual mean meridional circulation, hereafter residual circulation) and a mixing component (Garny et al., 2014). The residual circulation transports air masses from the tropical region towards the poles and creates the vertical and meridional gradients in the tracer' concentrations (Shepherd, 2007). The mixing consists in a two-way transport that occurs mostly on isentropic surfaces, hence, it is quasi-horizontal in the stratosphere (Shepherd, 2007). The residual circulation is mostly driven by the breaking of Rossby and planetary waves, hence it is the strongest during winter, i.e., when the breaking of these wave maximizes (Minganti et al., 2020). The BDC maintains the observed meridional and vertical temperature structure of the stratosphere (Holton, 2004), and strongly influences the stratospheric distribution of chemical tracers, like ozone and greenhouse gases (e.g., Butchart, 2014).

In the tropical stratosphere, one of the most important modes of variability is the Quasi Biennial Oscillation (QBO, Baldwin et al., 2001). The QBO consists in easterly (i.e., $u < 0$, E-QBO) and westerly (i.e., $u > 0$, W-QBO) zonal wind regimes that propagate downward in the tropical stratosphere, with a variable period from 20 to 37 months (Pascoe et al., 2005; Anstey et al., 2022). This irregular period is mainly driven by the variability in small scale (gravity wave) activity and, to a lesser extent, by variability in tropical upwelling (Kim, 2025). The QBO is not only restricted to the equatorial regions, but its impacts can reach the subtropical and even extratropical regions (i.e., teleconnections). In the tropical region, the QBO induces a temperature anomaly that is in thermal wind balance with the vertical wind shear (Baldwin et al., 2001). In order to maintain this thermal wind balance, a meridional circulation occurs in the Tropics and subtropics (i.e., the QBO secondary meridional circulation, hereafter secondary circulation, Plumb and Bell, 1982; Baldwin et al., 2001). Under conditions of descending easterlies (i.e., E-QBO), there is increased tropical upwelling that causes adiabatic warming and preserves the temperature maximum at the equator (Baldwin et al., 2001). Such increased upwelling is compensated by descent in the subtropics. The circulation pattern is completed by poleward motion at the levels of maximum easterly wind (i.e., usually located in the upper stratosphere) and by equatorward motion at the levels of maximum westerly winds (usually located in the lower stratosphere) (Choi et al., 2002). During descending westerly wind shears (i.e., W-QBO), an opposite circulation develops. The secondary circulation is substantially stronger in the winter hemisphere, especially the meridional and vertical velocities in the subtropics (Baldwin et al., 2001), and can also be significantly impacted by ozone changes through changes in heating (Hitchcock and Ming, 2025). The QBO impacts not only the tropical and subtropical regions, but also the extratropics through teleconnections. In particular, the wintertime northern polar vortex is weaker during the E-QBO phase and stronger during the W-QBO phase: this teleconnection is often referred to as the Holton-Tan effect (Holton and Tan, 1980). The mechanisms driving the Holton-Tan effect are still uncertain (Anstey et al., 2022; Butchart, 2022). One proposed mechanism is the poleward shift of the zero zonal

https://doi.org/10.5194/egusphere-2026-3449
Preprint. Discussion started: 25 June 2026


wind line in the winter subtropics. The zero zonal wind line acts as a waveguide and confines the extratropical planetary waves towards the higher latitudes, leading to a warmer and weaker vortex (Holton and Tan, 1980). Another proposed mechanism involves the QBO secondary circulation enhancing extratropical refraction of planetary waves (Garfinkel et al., 2012). Despite modeling studies investigating the origin of the Holton-Tan effect (e.g., Anstey and Shepherd, 2014), there is still no consensus on the dominant underlying mechanism (Anstey et al., 2022; Butchart, 2022). In addition, Yamazaki et al. (2020) proposed that QBO-induced tropospheric anomalies in convection can contribute to the Holton-Tan effect, which has in turn a strong influence on the tropospheric and surface climate at mid and high latitudes, e.g., on mean sea level pressure, temperature and snow cover (Gray et al., 2018; Kidston et al., 2015; Kumar et al., 2024).

In the past decade, the chemical and dynamical conditions of the stratosphere have been highly perturbed (Salawitch et al., 2025). In late 2018/2019 boreal winter, anomalous concentrations of $N_2O$ were first identified in the Northern Hemisphere (NH) mid-latitudes by Manney et al. (2022). That study proposed that the particular QBO phase during that period (together with the 2019 SSW) and its resulting modulation of stratospheric transport might be responsible for the $N_2O$ anomalies. Despite their magnitudes, the $N_2O$ anomalies in late 2018/2019 boreal winter in the northern mid-latitudes have not been extensively examined. In this study, we investigate these $N_2O$ anomalies that occurred in the NH in late 2018/2019 boreal winter, with the specific aim of quantifying their magnitude and identifying their dynamical and transport origins. Since this manuscript focuses on a specific event in the late 2018/2019 boreal winter, we will not use free-running models but observationally based products (e.g., reanalyses, specified-dynamics models and merged observational satellite datasets). Reanalysis datasets combine atmospheric observations with a global forecast model through data assimilation to provide a global multi-decadal and continuous state of the past atmosphere. Meteorological reanalyses assimilate dynamical observations such as surface pressure, wind and temperature and are often used to drive chemistry transport models (CTMs) to simulate realistic distributions of chemical species (e.g., Ménard et al., 2020). Chemical reanalyses assimilate chemical observations and their transport is driven by external meteorological fields (often obtained from meteorological reanalyses, Errera et al., 2019). Chemical reanalyses are often used to evaluate the evolution of the concentrations of chemical tracers in CTMs and climate models (e.g., Minganti et al., 2020; Chabrillat et al., 2025). Specified dynamics models usually constrain the dynamics of a chemistry climate model towards the dynamics of a meteorological reanalysis (e.g., Davis et al., 2022).

This manuscript follows up on the closely related works of Minganti et al. (2020, hereafter M2020) and Minganti et al. (2022, hereafter M2022). M2020 investigated the climatologies of the impact of transport on the $N_2O$ concentrations and its rates of change, and paved the way for studies of changes in stratospheric transport using $N_2O$ as a tracer. M2022 studied decadal changes (trends) of $N_2O$ concentrations in the stratosphere and related it to changes in the BDC. The present work aims to use the climatological groundwork of M2020 and the knowledge obtained in M2022 to study the extreme anomaly in $N_2O$ concentrations that occurred in late 2018/2019 boreal winter in the NH.

The manuscript is structured as follows. Section 2 describes the datasets used in this study and the method used to investigate the $N_2O$ anomalies. Section 3 shows time series at 50 hPa of $N_2O$ anomalies (together with transport-related quantities) in order to highlight the magnitude of the anomalies in late 2018/2019 boreal winter compared to the rest of the records. In Section

https://doi.org/10.5194/egusphere-2026-3449
Preprint. Discussion started: 25 June 2026


4, we focus on the anomalies in late 2018/2019 boreal winter over the NH. Section 5 discusses the dynamical causes of these anomalies. Section 6 summarizes and concludes the study.

## 2 Data and Method

In this Section, we describe the datasets used and the Transformed Eulerian Mean (TEM) diagnostics.

### 2.1 SWOOSH

The Stratospheric Water and OzOne Satellite Homogenized (SWOOSH, Davis et al., 2016) dataset is a merged record of satellite datasets that includes data from several limb-viewing instruments. The primary products in SWOOSH include vertical profiles of zonal and monthly means of ozone and water vapour concentrations on pressure levels (from 1 to 316 hPa). SWOOSH products are provided on several horizontal and vertical grids, but in this study we use the zonal-mean SWOOSH products with 5°latitude spacing on pressure levels.

In this study, we use a new merged $N_2O$ SWOOSH product, which is constructed using profiles from the Atmospheric Chemistry Experiment Fourier Transform Spectrometer (ACE-FTS, Bernath, 2017) and Aura Microwave Limb Sounder (MLS, Waters et al., 2006). Aura MLS $N_2O$ provides complete spatial sampling but contains drifts that render $N_2O$ unsuitable for long-term trends (Livesey et al., 2021), while ACE-FTS is deemed more stable but provides sparse sampling. These two products are combined in a way that preserves the long-term absolute values of ACE-FTS, with data gaps filled in using the MLS meridional anomaly structure on a month-by-month basis. The SWOOSH $N_2O$ product is publicly available as of version 2.8, which is used in this paper.

We also use the 5°latitude zonal mean ozone product from SWOOSH. The ozone product in SWOOSH benefits from more instruments compared to $N_2O$, although for the time period addressed here the merged record is dominated by Aura MLS. The variability of stratospheric ozone profiles from SWOOSH has been validated in several studies (e.g., Kuttippurath et al., 2024).

### 2.2 M2-GMI

The Modern-Era Retrospective analysis for Research and Application version 2 (MERRA-2 Gelaro et al., 2017) - Global Modeling Initiative (M2-GMI, Strode et al., 2019) is a multidecadal (1980 to 2019) simulation of atmospheric composition using NASA's full chemistry model GMI (Douglass et al., 2004; Duncan et al., 2007; Nielsen et al., 2017). The meteorology of M2-GMI is constrained by temperature, winds, and surface pressure from the MERRA-2 meteorological reanalysis. The chemical species in M2-GMI are not constrained by observations except indirectly via the assimilated meteorology in the MERRA2 driving reanalysis. The GMI chemical mechanism includes over 120 species and more than 400 reactions. The simulation was run at a horizontal resolution of approximately 50 km on 72 vertical layers between the Earth's surface and 0.01 hPa. The vertical resolution in the stratosphere is between 1 and 2 km depending on the altitude.

https://doi.org/10.5194/egusphere-2026-3449
Preprint. Discussion started: 25 June 2026


### 2.2.1 M2-SCREAM

The MERRA-2 Stratospheric Composition Reanalysis of Aura MLS (M2-SCREAM, Wargan et al., 2023) is a chemical reanalysis of stratospheric composition developed at NASA's Global Modeling and Assimilation Office. It uses a configuration of the Constituent Data Assimilation System (Wargan et al., 2020a, b; Weir et al., 2021, 2026), in which MLS version 4.2 stratospheric profiles of ozone, water vapor, hydrogen chloride (HCl), nitric acid ($HNO_3$) and $N_2O$ are assimilated into the Goddard Earth Observing System (GEOS) atmospheric general circulation model coupled with the stratospheric chemistry mechanism StratChem (Nielsen et al., 2017, and references therein). Temperature, winds, surface pressure and tropospheric water vapor are constrained by the MERRA-2 meteorological reanalysis using the replay methodology (Orbe et al., 2017). In addition to MLS, total column ozone data from the Ozone Monitoring Instrument (Levelt et al., 2006, 2018) is also assimilated. Similarly to M2-GMI, M2-SCREAM is run at a horizontal resolution of approximately 50 km on 72 vertical layers, and covers the period between September 2004 and December 2024. M2-SCREAM $N_2O$ product is constrained by assimilated MLS observations between 68 hPa and 0.46 hPa. Version 4.2 MLS $N_2O$ suffers from a spurious negative drift in the lower stratosphere after 2010 (Livesey et al., 2021). While this makes M2-SCREAM $N_2O$ unsuitable for studies of long-term trends, its utility as a metric for interannual variability of transport has been demonstrated (Salawitch et al., 2025; Wargan et al., 2023).

## 2.3 BASCOE CTM simulations

We performed three simulations using the Belgian Assimilation System for Chemical ObsErvations CTM (BASCOE CTM, Errera et al., 2008). Each BASCOE CTM simulation is driven by one of the following three meteorological reanalyses: the European Center for Medium-Range Weather Forecast (ECMWF) fifth Reanalysis (ERA5, Hersbach et al., 2020), the Japanese Reanalysis for Three Quarters of a Century (JRA3Q, Kosaka et al., 2024) and MERRA-2 (Gelaro et al., 2017). These BASCOE CTM simulations driven by the meteorological reanalyses MERRA-2, ERA5 and JRA-3Q are indicated here as BASCOE-MERRA2, BASCOE-ERA5 and BASCOE-JRA3Q, respectively. The BASCOE CTM advects around 60 chemical species using a flux-form semi-Lagrangian scheme (Lin and Rood, 1996) and solves approximately 200 chemical reactions using a chemical kinetic preprocessor (Damian et al., 2002). The BASCOE CTM was run on a reduced horizontal grid of 2°x 2.5°, and a vertical grid that was adjusted for each reanalysis to limit the number of tropospheric levels where chemistry is not computed in BASCOE, while maintaining a high resolution in the upper layers, with a model top at around 0.01 hPa (Vervalcke et al., 2026). This approach reduces computational cost while ensuring accurate transport. The model was run on 49 vertical levels for MERRA2, 61 vertical levels for ERA5 and 53 vertical levels for JRA-3Q. All simulations were initialized in January 1997 using output from a BASCOE CTM simulation driven by ERA5 and terminated in December 2023. More information regarding the simulation setup and the driving reanalyses can be found in Vervalcke et al. (2026) and references therein.

## 2.4 BRAM2

This study uses the $N_2O$ product from the BASCOE reanalysis of Aura MLS version 2 (BRAM2, Errera et al., 2019). The BRAM2 chemical reanalysis is driven by the meteorology from the ECMWF Interim Reanalysis (ERA-Interim, here-

https://doi.org/10.5194/egusphere-2026-3449
Preprint. Discussion started: 25 June 2026


after ERAI, Dee et al., 2011), and covers the period from August 2004 to August 2019. BRAM2 is produced on a 3.75°x 2.5°(longitude-latitude) horizontal resolution, with 37 vertical levels, 25 of which are above 100 hPa. BRAM2 assimilates several chemical species from Aura MLS version 4.2 observations, including $N_2O$ standard product from the 190 GHz radiometer. MLS $N_2O$ has a vertical range of validity between 68 and 0.46 hPa, where this species is assimilated in BRAM2. BRAM2 $N_2O$ has been evaluated against several independent observations (ACE-FTS and the Michelson Interferometer for Passive Atmospheric Sounding, MIPAS, Fischer et al., 2008). Below 3 hPa, BRAM2 agrees well with ACE-FTS ($\pm 10\%$) and MIPAS ($\pm 15\%$). Above that level, BRAM2 is poorly characterized showing larger differences against these instruments. BRAM2 $N_2O$ is thus recommended for scientific use between 68 and 3 hPa. BRAM2 $N_2O$ displays also the negative drift that characterizes MLS version 4.2 $N_2O$, ranging from 5 to 15%, with a maximum in the lower stratosphere (Errera et al., 2019; Livesey et al., 2021). This drift, which similarly affects M2-SCREAM, does not pose a problem for this study because linear trends are removed prior to the computation of anomalies.

### 2.5 SD-WACCM

We use a specified dynamics (SD) simulation from the Community Earth System Model (CESM, Danabasoglu et al., 2020) version 2.2.0 with the Whole Atmosphere Community Climate Model (WACCM, Gettelman et al., 2019) version 6 as its atmospheric component (SD-WACCM, Orbe et al., 2020; Yu et al., 2022). The simulation was performed with a horizontal resolution of 1.9°latitude x 2.5°longitude and uses the middle atmospheric chemistry scheme, with the dynamics nudged to MERRA-2 meteorology (i.e., component set FWmaSD). Davis et al. (2023a) showed that this middle atmospheric chemistry scheme, which is simplified primarily in the troposphere, is appropriate for stratospheric studies. Although long-term residual circulation changes are in general not well represented in SD simulations, they are generally expected to be more reliable than their free-running counterparts in reproducing intraseasonal to interannual variability of long-lived trace gases such as $N_2O$ (Davis et al., 2022; Chrysanthou et al., 2019; Davis et al., 2023b).

### 2.6 TEM

For stratospheric tracers, the TEM diagnostics (Andrews et al., 1987) allows separating the impact of transport and chemistry on the zonal mean local rate of change of a tracer with mixing ratio $\chi$:

$$\overline{\chi}_t = -\bar{v}^*\overline{\chi}_y - \bar{w}^*\overline{\chi}_z + e^{z/H}\nabla\cdot\mathbf{M} + \overline{S} + \bar{\epsilon}, \tag{1}$$

where $\chi$ represents $N_2O$ concentrations, $\mathbf{M} = -e^{-z/H}(\overline{v'\chi'} - \overline{v'\theta'}\bar{\chi}_z/\bar{\theta}_z, \overline{w'\chi'} + \overline{v'\theta'}\bar{\chi}_y/\bar{\theta}_z)$ is the eddy flux vector, and $(\bar{v}^*, \bar{w}^*)$ are the meridional and vertical components of the residual circulation, respectively. Overbars denote zonal means and prime quantities indicate deviations from it, while subscripts indicate partial derivatives. $H = 7$ km is the scale height, and $z \equiv -Hlog_e(p/p_s)$ is the log-pressure altitude, with the surface pressure $p_s = 10^5$ Pa. The $S$ term is the net rate of change due to chemistry, defined as the difference between the production ($\bar{P}$) and loss ($\bar{L}$) rates $\bar{S} = \bar{P} - \bar{L}$. The $\bar{\epsilon}$ contribution represents the residual of the budget, i.e., the difference between the actual rate of change of $\overline{\chi}$ and the sum of the transport and chemistry terms on the right-side hand of Eq. 1.

https://doi.org/10.5194/egusphere-2026-3449
Preprint. Discussion started: 25 June 2026


The transport terms in Eq. 1 can be grouped as follows:

$$\bar{\chi}_t = A_y + M_y + A_z + M_z + (\bar{P} - \bar{L}) + \bar{\epsilon}, \tag{2}$$

where:

$$A_y = -\bar{v}^* \bar{\chi}_y, \tag{3a}$$
$$M_y = e^{z/H} cos\phi^{-1} (M^{(y)} cos\phi)_y, \tag{3b}$$
$$A_z = -\bar{w}^* \bar{\chi}_z, \tag{3c}$$
$$M_z = e^{z/H} (M^{(z)})_z, \tag{3d}$$

with $A_y$ representing the impact of meridional residual advection on the $N_2O$ concentrations, $M_y$ that of the horizontal transport due to eddy mixing, $A_z$ that of the vertical residual advection and $M_z$ that of the vertical eddy mixing (all expressed in ppbv/day). We refer to M2020 for a more detailed description of the TEM framework applied to the $N_2O$ mixing ratios in the stratosphere and for a comprehensive discussion of the contribution of each term to the $N_2O$ budget.

In order to better interpret the $N_2O$ TEM budget, we also compute the Eliassen-Palm Flux Divergence (EPFD). The Eliassen-Palm flux is a 2-D vector defined as $\mathbf{F} \equiv (F^{(\phi)}, F^{(z)})$ (Andrews et al., 1987), with its meridional and vertical components given respectively by:

$$F^{(\phi)} \equiv e^{-z/H} acos\phi(\bar{u}_z \overline{v'\theta'}/\overline{\theta_z} - \overline{v'u'}), \tag{4a}$$
$$F^{(z)} \equiv e^{-z/H} acos\phi\{[f - (acos\phi)^{-1}(\bar{u}cos\phi)_\phi]\overline{v'\theta'}/\overline{\theta_z} - \overline{w'u'}\}. \tag{4b}$$

The EPFD is a measure of the dynamical forcing from resolved waves (i.e., planetary waves) on the mean flow (Edmon Jr et al., 1980):

$$EPFD = \nabla \cdot \mathbf{F} = EPFD_y + EPFD_z, \tag{5}$$

with $EPFD_y$ and $EPFD_z$ defined as:

$$EPFD_y \equiv -(\rho_0 \overline{v'u'})_y, \tag{6a}$$
$$EPFD_z \equiv (\rho_0 f_0 \overline{v'\theta'}/\overline{\theta}_z)_z. \tag{6b}$$

## 3 Exceptional characteristics of the late 2018/2019 boreal winter

In this Section, we show the characteristics of the late 2018/2019 boreal winter in the context of the recent climate record in terms of tracer and transport anomalies. Figure 1 shows latitudinal profiles of $N_2O$ and ozone concentrations obtained from SWOOSH at 50 hPa for February 2019, along with latitudinal profiles for the rest of the SWOOSH record. In the lower stratosphere, the ozone concentrations are mostly determined by transport (Chipperfield et al., 2018; Ball et al., 2019), as their

https://doi.org/10.5194/egusphere-2026-3449
Preprint. Discussion started: 25 June 2026


chemical lifetime is of the order of months or even years, since the solar radiation is not sufficient to drive photochemistry in the lower stratosphere (Brasseur and Solomon, 2005). Hence, we also show ozone concentrations to highlight the impact of transport on determining not only the $N_2O$ anomalies, but also other tracers anomalies. We show results at 50 hPa because that is the pressure level where the tracer anomalies are the largest (Salawitch et al., 2025). As shown already by Manney et al. (2022) and Salawitch et al. (2025), Fig. 1 indicates that the $N_2O$ concentrations are anomalously large in the NH in February 2019. These $N_2O$ anomalies are accompanied by negative ozone anomalies over the same stratospheric region and period. Both the $N_2O$ and the ozone anomalies in the NH in February 2019 are record-breaking in the SWOOSH dataset. The opposite sign in the ozone and $N_2O$ anomalies is consistent with their anti-correlation in the lower stratosphere at extratropical latitudes (Hegglin and Shepherd, 2007). Contrarily to the NH, no anomaly in $N_2O$ nor ozone was observed in the Southern Hemisphere (SH) in February 2019.

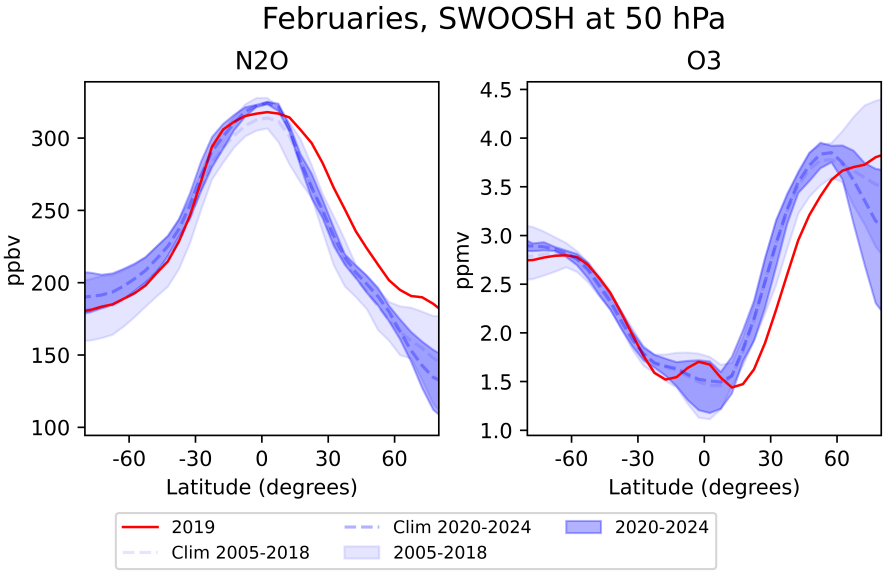


**Figure 1.** Latitudinal profiles of $N_2O$ concentrations (ppbv, left) and ozone concentrations (ppmv, right) at 50 hPa for SWOOSH. The red line indicates February 2019. The light dashed blue line indicates the mean $N_2O$ and ozone concentrations for the Februaries between 2005 and 2018. The dark dashed blue line indicates the mean $N_2O$ and ozone concentrations for the Februaries between 2020 and 2024. The shadings indicate the minimum/maximum values of the tracer's concentrations for the two periods mentioned above.

In the rest of the Section, we show time series of anomalies of stratospheric tracers ($N_2O$ and ozone), together with anomalies of the $A_y$ term of the $N_2O$ TEM budget and of the $EPFD_z$. Anomalies are computed as the difference between the monthly time series and their mean climatological value of each month. We also scale the anomalies by their respective standard deviation to have the same units (i.e., sigmas) and compare the respective magnitudes of the tracers, the $A_y$ and the $EPFD_z$ terms. Since we do not aim to investigate trends, we remove the linear trend from the anomalies time series by fitting a simple

https://doi.org/10.5194/egusphere-2026-3449
Preprint. Discussion started: 25 June 2026


linear term. Section 3.1 presents time series of anomalies of $N_2O$ and ozone, Section 3.2 shows time series of anomalies of $A_y$, and Section 3.3 the time series of $EPFD_z$ anomalies.

### 3.1 Time series of tracer anomalies

Figure 2 shows time series of $N_2O$ anomalies over the northern mid-latitudes (30°N to 60°N) at 50 hPa. The datasets generally agree well among each other and the $N_2O$ anomalies tend to oscillate between -2 and 2 sigmas and occasionally reach 3 sigmas. Regarding the timing of the $N_2O$ anomalies, the datasets generally agree well in the considered record. This indicates a good representation of the frequency and duration of the anomalies in the stratospheric transport of $N_2O$, which consists mainly in the meridional transport at these latitudes and pressure level (M2020). On the other hand, the amplitude of the $N_2O$ anomalies varies among the datasets (e.g., in BASCOE-MERRA2). The differences in the amplitudes of the $N_2O$ anomalies indicate differences in the strength of the stratospheric transport of $N_2O$, which is related to the accuracy of each dataset in resolving and transporting horizontal and vertical $N_2O$ gradients (see Sect. 2.6). Because of that, some of the differences in Fig. 2 can be partly explained by differences in spatial resolution of the datasets (both horizontal and especially vertical). Nevertheless, the different spatial resolutions between the datasets alone cannot explain the differences in the $N_2O$ anomalies, and the nature of each dataset plays a major role in determining these differences.

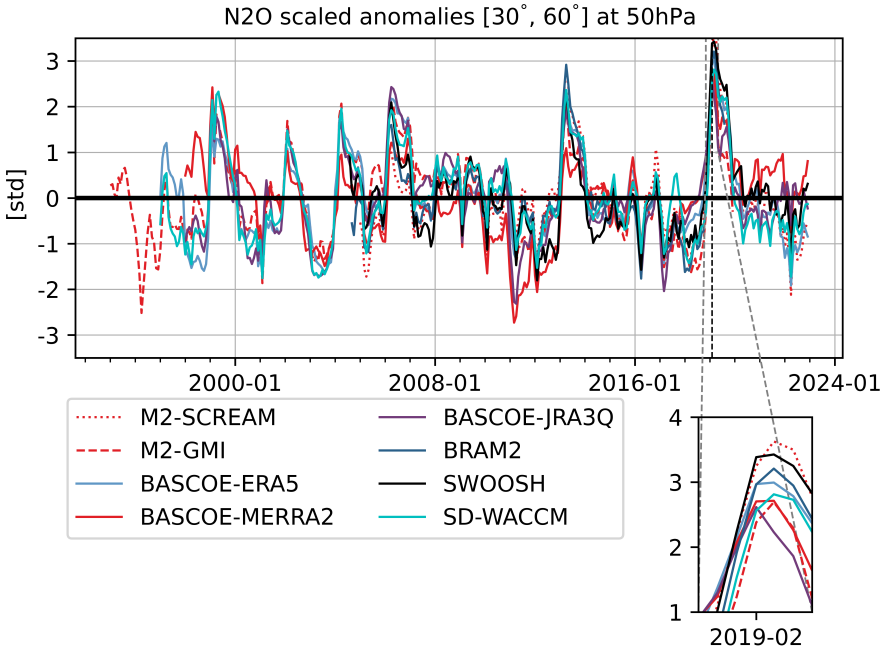


**Figure 2.** Time series of anomalies of the de-trended $N_2O$ concentrations scaled by their standard deviations at 50 hPa averaged between 30°-60°N. The vertical dashed black line indicates February 2019. The color code is in the legend. The vertical axis is in units of standard deviations.

https://doi.org/10.5194/egusphere-2026-3449
Preprint. Discussion started: 25 June 2026


The BASCOE-MERRA2 simulation differs from the other datasets in some parts the period considered here. It simulates smaller amplitudes of the $N_2O$ anomalies in periods when the other datasets show larger $N_2O$ anomalies (e.g., early 2002, early 2004). From 2008 to 2013, BASCOE-MERRA2 shows the opposite behaviour, with larger negative amplitudes of the $N_2O$ anomalies, when the other datasets show smaller anomalies (in 2011 together with BASCOE-JRA3Q). In early 2013, BASCOE-MERRA2 show also large differences compared to the other datasets, with smaller amplitudes of the $N_2O$ positive anomalies, and provides larger amplitudes of the positive $N_2O$ anomalies after 2020. Overall, BASCOE-MERRA2 generally tends to deliver smaller amplitudes (i.e., less positive/less negative) of the $N_2O$ anomalies compared to the other datasets. This underestimation occurs also with respect to the other MERRA2-based datasets (i.e., M2-GMI, M2-SCREAM and SD-WACCM). Surprisingly, these other MERRA2-based datasets agree more with the datasets based on other meteorological reanalyses (BASCOE-ERA5, BASCOE-JRA3Q, BRAM2, SWOOSH) than with BASCOE-MERRA2. This discrepancy indicates that BASCOE-MERRA2 suffers from particular features that deteriorate its simulation of $N_2O$ transport in this region. In the lower stratospheric mid-latitudes, the $N_2O$ concentrations are inversely proportional to the mean Age of Air (mAoA, M2020). Hence, the smaller magnitudes of the $N_2O$ anomalies are consistent with the recent mAoA results from Vervalcke et al. (2026), who found that MERRA2 delivers the oldest mAoA compared to ERA5 and JRA3Q using the same BASCOE CTM simulations.

The comparison between the chemical reanalyses BRAM2 and M2-SCREAM generally delivers very good agreement, with a few differences at specific times of the record. Notably, in early 2005, M2-SCREAM shows a negative $N_2O$ anomaly that is not present in BRAM2 (nor in the other datasets). Other small differences between the two chemical reanalyses occur later on with slightly larger amplitudes in M2-SCREAM compared to BRAM2. Wargan et al. (2023) showed good agreement between the $N_2O$ climatologies of BRAM2 and M2-SCREAM, with the largest differences at mid-latitudes below the lowermost validity level for BRAM2 (i.e., 68 hPa). They did not show comparison of $N_2O$ anomalies between M2-SCREAM and BRAM2, but our results at 50 hPa (with little differences between the two datasets) are consistent with their results for the $N_2O$ climatologies. Wargan et al. (2023) showed $N_2O$ anomalies at around 50 hPa (their Fig. 13), and the $N_2O$ anomaly in early 2019 at mid-latitudes is present in their figure, but no explanation was given at that stage.

In early 2013, a large positive $N_2O$ anomaly occurred, similar to the anomaly in early 2019, but with smaller amplitude. This anomaly was shown in Wargan et al. (2023), but not investigated in detail. Manney et al. (2022) also shows the 2013 and 2019 anomalies and suggests a connection with the QBO phase. We will show later that the 2013 and 2019 $N_2O$ anomalies were preceded by very different transport and dynamical anomalies.

Across all datasets, the largest $N_2O$ anomaly occurs in early 2019 (February and March). In these months, the $N_2O$ anomalies reach large positive values of 2.5 sigmas in the BASCOE-JRA3Q, BASCOE-MERRA2 and M2-GMI and 3 sigmas in BASCOE-ERA5, SWOOSH, BRAM2 and M2-SCREAM. SD-WACCM reproduces well the positive $N_2O$ anomalies, with values close to those of SWOOSH and the CTM simulations. We notice that the datasets that assimilate $N_2O$ concentrations (BRAM2 and M2-SCREAM) or directly measure them (SWOOSH) provide the largest $N_2O$ anomalies. BASCOE-ERA5 delivers $N_2O$ anomalies larger than the other CTM simulations and closer to the MLS-based datasets. M2022 showed that the ECMWF reanalyses provided the most realistic $N_2O$ interannual variability compared to MERRA2 and JRA-55. The results

https://doi.org/10.5194/egusphere-2026-3449
Preprint. Discussion started: 25 June 2026


for the $N_2O$ anomalies shown here confirm that ERA5 produces realistic variability for $N_2O$, both decadal and interannual. The other datasets (BASCOE-MERRA2, BASCOE-JRA3Q, M2-GMI and SD-WACCM) slightly underestimate the $N_2O$ anomalies at 50 hPa at mid-latitudes in these early 2019 months. In the NH, the average mAoA in ERA5 is larger than in the observational datasets (Ploeger et al., 2021). Given the inverse relationship between $N_2O$ and mAoA, this discrepancy in mAoA is consistent with the smaller $N_2O$ anomalies in the BASCOE-ERA5 compared to the MLS-based observational datasets shown in this study. Interestingly, the mAoA derived from ERAI in the NH is younger than that calculated from observational datasets (Ploeger et al., 2021). However, BRAM2 (driven by ERAI winds) does not show a corresponding larger $N_2O$ anomalies. This is because the $N_2O$ concentrations in BRAM2 are constrained by the assimilation of MLS observations.

The smaller $N_2O$ anomalies in SD-WACCM in early 2019 compared to MLS-based datasets are consistent with the underestimation of the $N_2O$ variability in WACCM4(CESM1) compared to MLS itself (but over a different period, Froidevaux et al., 2019). In the NH mid-latitudes, Garny et al. (2024) found a larger amplitude of the mAoA anomalies in the lower stratosphere in the reanalyses compared to climate models. The SD-WACCM simulation shown here does not produce significantly smaller amplitudes of $N_2O$ anomalies for a similar stratospheric region. This indicates that the nudging towards the MERRA2 dynamics successfully modifies the WACCM $N_2O$ anomalies towards more realistic values. The good representation of variability in SD-WACCM (here expressed with $N_2O$ anomalies) is confirmed also by Yu et al. (2022), who evaluated the water vapour variability in the tropical region and reported realistic trends in water vapour in SD-WACCM compared to merged satellite datasets.

Figure 3 shows time series of ozone anomalies at 50 hPa averaged over the same latitude band as the $N_2O$ anomalies in Figure 2. Decadal trends in ozone in the lower stratosphere in the mid-latitudes are a subject of current research, as there are significant discrepancies between model simulations and observations (WMO, 2022; Benito-Barca et al., 2025). Hence, (as done for the $N_2O$ anomalies) we detrend the ozone concentrations before computing their anomalies in order to exclude possible impact from ozone trends. The $N_2O$ and ozone concentrations are anti-correlated in the lower stratosphere at extratropical latitudes because of stratospheric transport (Hegglin and Shepherd, 2007). At these latitudes and pressure levels in the stratosphere, the climatological transport is directed northward, with consequent increase of $N_2O$ concentrations (transported in the tropical stratosphere from the troposphere, M2020), and decrease in ozone (produced in the tropical stratosphere, Abalos et al., 2013). Hence, negative ozone anomalies correspond to positive $N_2O$ anomalies, and both occur during boreal winter, when stratospheric transport is the strongest (Birner and Bönisch, 2011). For example, the positive $N_2O$ anomalies in early 2004 and 2006 correspond to negative ozone anomalies in the same periods. Larger positive $N_2O$ anomalies (e.g., early 2013) also correspond to larger negative ozone anomalies.

All datasets agree quite well among each other. The timing and magnitudes of the largest ozone anomalies are consistent among the datasets with a few exceptions. Notably, the BASCOE-JRA3Q, BASCOE-MERRA2 and M2-GMI simulations occasionally show larger magnitudes of the ozone anomalies (e.g., negative in early 2000 for BASCOE-MERRA2, positive in early 2003 for M2-GMI and negative in early 2008 for BASCOE-JRA3Q). These discrepancies correspond to similar differences in the $N_2O$ anomalies (with the opposite sign) in Fig. 2. This correspondence highlights the prominent role of transport in determining the ozone (and $N_2O$) concentrations in this region. On the other hand, in early 2010 all datasets show con-

https://doi.org/10.5194/egusphere-2026-3449
Preprint. Discussion started: 25 June 2026


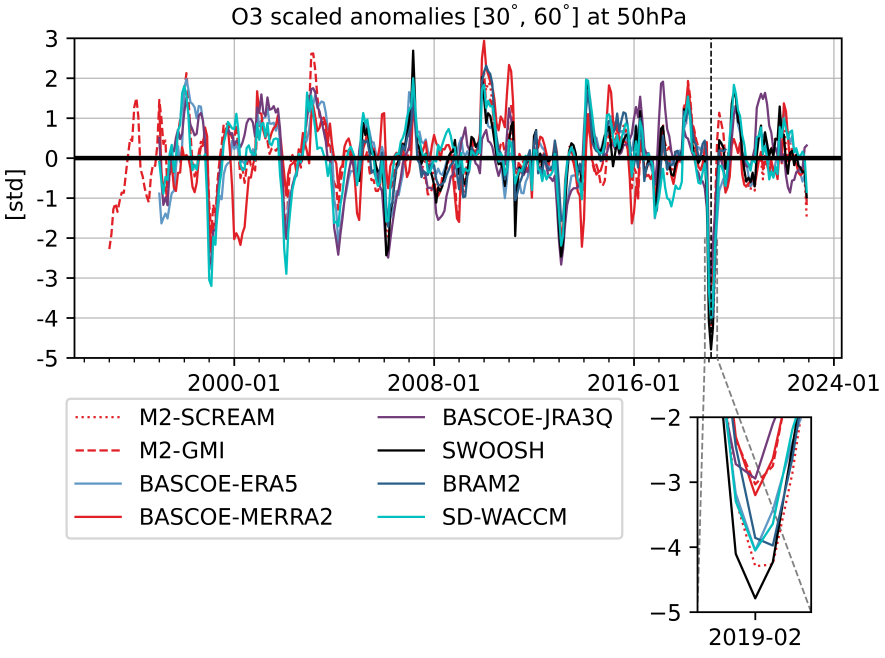


**Figure 3.** As Fig. 2, but for ozone.

sistent positive ozone anomalies (reaching 3 sigmas in BASCOE-MERRA2) that do not correspond to equally large negative $N_2O$ anomalies for the same period. This discrepancy between ozone and $N_2O$ anomalies is related to the origin of the ozone anomalies in 2010. These large positive ozone anomalies in 2010 originated from an unusually pronounced negative phase of the Arctic Oscillation and North Atlantic Oscillation (Steinbrecht et al., 2011), which did not substantially affect $N_2O$ (Fig. 2).

The largest negative ozone anomaly in the record (i.e., in late 2018/2019 boreal winter) coincides with the largest $N_2O$ positive anomaly shown in Fig. 2. In early 2019, in particular in February, the negative ozone anomalies reach and exceed 3 sigmas (for BASCOE-JRA3Q, BASCOE-MERRA2 and M2-GMI) and 4 sigma (for BASCOE-ERA5, SWOOSH, BRAM2, M2-SCREAM and SD-WACCM). As for the $N_2O$ anomalies, all datasets agree well both on the timing and on the exceptional magnitude of these ozone anomalies in February 2019. In addition, the differences in the amplitudes of the ozone anomalies are consistent with the differences in the amplitudes of the $N_2O$ anomalies. M2-GMI, BASCOE-MERRA2 and BASCOE-JRA3Q deliver the smallest amplitudes for both ozone and $N_2O$ in February 2019, while SWOOSH, M2-SCREAM and BRAM2 provide the largest amplitudes for both $N_2O$ and ozone. The ozone anomalies in BASCOE-ERA5 and SD-WACCM are closer to the chemical reanalyses and SWOOSH compared to the $N_2O$ anomalies for the same period.

Both Figures 2 and 3 provide strong evidence that the $N_2O$ and ozone anomalies in February 2019 in the northern mid-latitudes at 50 hPa were driven by transport. In the rest of the manuscript, we will show only $N_2O$ results because $N_2O$ has no significant chemical reactions in the whole stratosphere at mid-latitudes. In addition, we will show that large $N_2O$ anomalies are not limited to the lower stratosphere, but they occur also at higher levels (e.g., at 15 hPa, see Fig. S1). In the upper stratosphere,

https://doi.org/10.5194/egusphere-2026-3449
Preprint. Discussion started: 25 June 2026


ozone undergoes chemical reactions that limit our capacity to understand the impact of transport on its concentrations (Brasseur and Solomon, 2005). As a consequence, the ozone anomalies at the upper levels (e.g., at 15 hPa) are not as pronounced as in the lower stratosphere (Fig. S2).

### 3.2 Time series of $A_y$ anomalies

Figure 4 shows time series of anomalies of the $A_y$ term, i.e., the term of the $N_2O$ TEM budget that quantifies the impact of the meridional residual advection on the $N_2O$ concentrations. We show anomalies of the $A_y$ term because the amplitudes of the anomalies of the other $N_2O$ TEM terms in the 2018/2019 boreal winter are much smaller (see Supplement, Figs. S3-S6). As in Figs. 2 and 3, the $A_y$ anomalies are detrended and normalised by their standard deviations for each dataset. Contrarily to Figs. 2 and 3, SWOOSH is not shown because it is not possible to compute its $N_2O$ TEM budget from satellite observational data. In the lower stratospheric mid-latitudes, the climatological $A_y$ is positive in boreal winter, indicating the wintertime poleward residual advection due to the BDC (M2020). Hence, positive (negative) $A_y$ anomalies (on top of the positive climatological $A_y$) indicate that the residual meridional advection of $N_2O$ was enhanced (weakened) over that region.

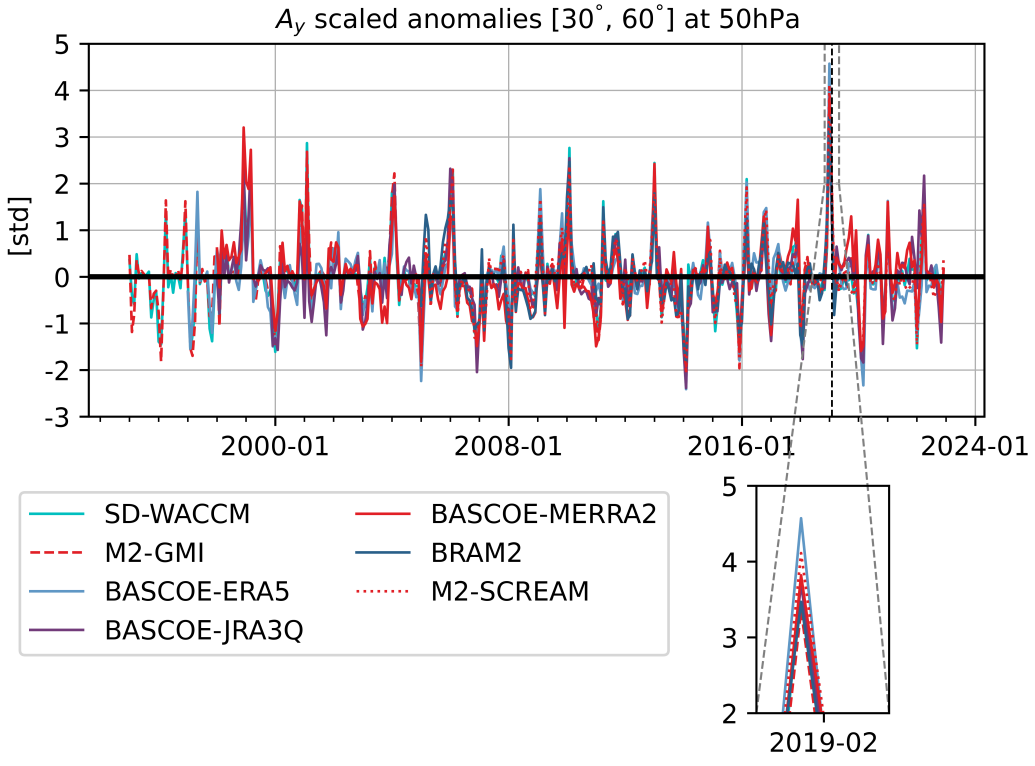


**Figure 4.** As Fig. 2, but for the $A_y$ term. SHOOSH is not shown.

https://doi.org/10.5194/egusphere-2026-3449
Preprint. Discussion started: 25 June 2026


Across the whole period, the $A_y$ anomalies generally agree among the datasets and rarely exceed 3 sigma. Occasionally, BRAM2 shows larger amplitudes of the $A_y$ anomalies compared to the other datasets (e.g., early 2005 and 2009). These larger amplitudes in BRAM2 do not correspond to similar features in M2-SCREAM, indicating that the different winds driving the two reanalyses are the main reason of the differences. Indeed, differences in stratospheric transport between ERAI and MERRA2 have been reported using age of air (Chabrillat et al., 2018; Ploeger et al., 2019), the $N_2O$ TEM budget (M2020), and ozone (Davis et al., 2023b). Another possible reason for the differences between BRAM2 and M2-SCREAM is their different vertical and horizontal resolutions. BRAM2 has a coarser vertical and horizontal resolutions compared to M2-SCREAM, which impacts the computation of the meridional and vertical gradients in the $A_y$ term.

Across all the dataset record, early 2019 stands out: the $A_y$ anomalies are positive and largely exceed 3 sigmas for SD-WACCM, M2-GMI, BASCOE-JRA3Q, BASCOE-MERRA2 and BRAM2 and reach 4 sigma for M2-SCREAM and BASCOE-ERA5. These $A_y$ anomalies occur approximately one month before the $N_2O$ anomalies shown in Fig. 2 (i.e., in January 2019). This time lag between the $A_y$ and $N_2O$ anomalies is expected because the $N_2O$ concentrations are a cumulative quantity, while the $A_y$ term is an instantaneous quantity that (by construction) contributes to the local $N_2O$ rate of change and ultimately to the $N_2O$ concentrations. The good agreement of SD-WACCM with the other datasets for the interannual variability of $A_y$ is not surprising: M2022 showed that the free-running version of CESM2/WACCM6 reproduced well the decadal changes of the $A_y$ ($+A_z$) term in the lower stratosphere at northern mid-latitudes compared to BASCOE-ERA5. The BASCOE-ERA5 simulation shows the largest $A_y$ anomaly in January 2019, indicating the strongest impact from the meridional residual advection on the $N_2O$ concentrations. In the northern mid-latitudes, ERA5 delivers slower mean BDC (quantified with mAoA) compared to ERAI, and comparable to MERRA2 (Ploeger et al., 2021; Diallo et al., 2021). This slower mean BDC does not necessarily contradict our findings of stronger $A_y$ anomalies in January 2019, because the seasonal cycle (i.e., the largest contribution to the mean $A_y$ term, M2020) has been removed in the computation of the $A_y$ anomalies. Concerning BASCOE-JRA3Q, Kobayashi and Iwasaki (2024) showed that the mean BDC intensity (quantified there with the tropical upwelling) is weaker in JRA3Q compared to ERA5 in boreal winter. This difference is consistent with the larger anomaly in the $A_y$ term in BASCOE-ERA5 compared to BASCOE-JRA3Q in January 2019.

For each dataset, the magnitudes of the $A_y$ anomalies do not always correspond to the magnitudes of the corresponding $N_2O$ anomalies in early 2019. BASCOE-ERA5 shows larger $A_y$ anomalies compared to M2-SCREAM in January, but smaller $N_2O$ anomalies in February. This discrepancy can be attributed to the anomalies in the vertical residual advection ($A_z$), which are stronger in M2-SCREAM compared to BASCOE-ERA5 (Fig. S4), in determining the final $N_2O$ anomaly. As a result, the anomalies in the total residual advection (i.e., $A_y + A_z$) in M2-SCREAM are larger compared to BASCOE-ERA5 (Fig. S5). Similar considerations can be done for M2-GMI and BRAM2. The BASCOE-MERRA2 and BASCOE-JRA3Q simulations simulate rather consistent magnitudes of the anomalies in $A_y$ and $N_2O$ concentrations. SD-WACCM is an exception because it shows one of the largest anomalies in the total advection term ($A_y + A_z$, Fig. S5), but it does not simulate the largest $N_2O$ anomalies. This discrepancy is likely due to the differences in the anomalies of the residual term (that includes sub-scale effects and numerical errors) between the datasets (Fig. S6). The anomalies in the residual term are near-zero in SD-WACCM and are different from zero in the other datasets, i.e., generally within 1 sigma except for M2-SCREAM and BRAM2 that reach

https://doi.org/10.5194/egusphere-2026-3449
Preprint. Discussion started: 25 June 2026


1.5 sigma (Fig. S6). The larger anomalies in the residual term in M2-SCREAM and BRAM2 are consistent with M2020, who showed that chemical assimilation results in larger residual terms compared to CTM experiments.

From our analysis, it is clear that the anomalies in the $N_2O$ concentrations are driven by anomalies of transport via its residual meridional advection. This becomes even more evident when looking at the anomalies of $\bar{v}^*$ (Fig. S7), which are consistent with the anomalies in $A_y$ in both timing and magnitude. Assuming little impact from sub-grid processes and steady-state mean flow, the meridional residual transport is mainly forced by the EPFD (Eq. 12.7 of Holton, 2004). Hence, we expect that anomalies in meridional residual advection (that ultimately drive the $N_2O$ anomalies) are driven by anomalies in the EPFD. In the next Section, we will show anomalies of the vertical component of the EPFD (i.e., $EPFD_z$) and relate them to the $A_y$ anomalies.

### 3.3 Time series of $EPFD_z$ anomalies

Figure 5 shows time series of the detrended anomalies of $EPFD_z$ scaled by their standard deviations (as previous figures). We show only the vertical component of the EPFD, i.e., $EPFD_z$, because its meridional component $EPFD_y$ does not present large anomalies in late 2018/2019 winter (see Fig. S8). In this Section, we show the convergence of $EPFD_z$ (i.e., -$EPFD_z$), because it drives the forcing from planetary waves, while the divergence of the EP flux inhibits it (Holton, 2004). In this way, positive (negative) anomalies indicate enhanced (inhibited) forcing from the breaking of planetary waves. In the following, we will show only the meteorological reanalyses that drive the CTM simulations and the chemical reanalyses (i.e., JRA3Q, MERRA2, ERAI and ERA5) together with SD-WACCM.

The timing of the $EPFD_z$ anomalies agrees remarkably well among the datasets, but their magnitudes can vary. SD-WACCM tends to simulate slightly larger magnitudes of the $EPFD_z$ anomalies, both positive and negative (e.g., early 1998, 1999, 2006, 2010, 2018). M2020 showed that the free-running configuration of the previous WACCM version (CESM1/WACCM4) simulates smaller climatological EPFD in a similar region. This discrepancy between the free-running and specified-dynamics WACCM configurations indicates that the nudging towards MERRA2 meteorology plays a role in determining the planetary wave forcing in WACCM. In addition, this difference between the free-running and SD configurations is consistent with Davis et al. (2022), who showed that the frequency of the nudging towards the MERRA2 meteorology impacts the planetary wave forcing by reducing the globally-averaged errors in the EPFD.

In early 1999, large anomalies of the $EPFD_z$ occur, reaching and exceeding 3 sigmas. These anomalies correspond to positive anomalies in $N_2O$ and in the $A_y$ term and to negative anomalies in ozone, suggesting a dynamical origin. Even though the $EPFD_z$ anomalies in early 1999 are record-breaking, they do not correspond to equally large anomalies in $N_2O$ or ozone concentrations, nor in the $A_y$ term. In addition, MLS data were not available at that time, and this lack of observational data reduces our capability to evaluate that period. For these reasons, we do not investigate the $EPFD_z$ anomalies in early 1999 in detail.

In January 2019, the positive $EPFD_z$ anomalies indicate an enhanced wave breaking compared to the rest of the period. All datasets agree with an increase of around 2.3 to 2.6 standard deviations above the average, with SD-WACCM and ERA5 providing the largest $EPFD_z$ anomalies and JRA3Q and MERRA2 showing smaller amplitudes. ERAI provides the smallest

https://doi.org/10.5194/egusphere-2026-3449
Preprint. Discussion started: 25 June 2026


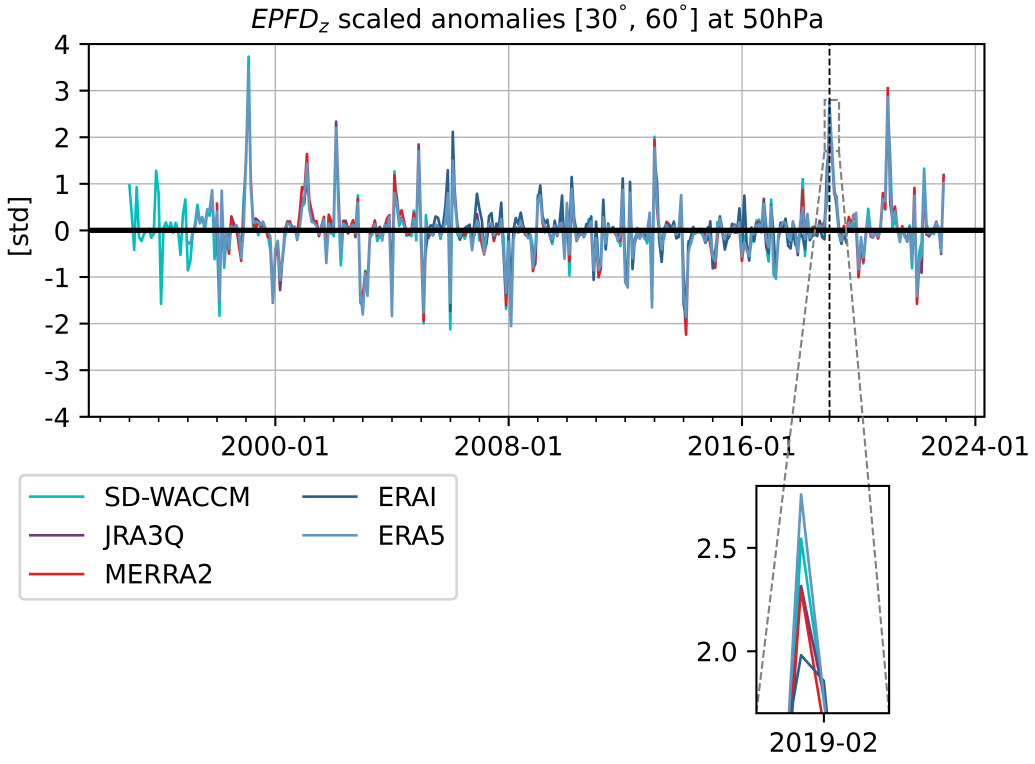


**Figure 5.** As Fig. 2, but for -$EPFD_z$ (see text for details).

$EPFD_z$ anomalies and do not reach 2 sigma. This difference between ERAI and the other datasets can be attributed to the coarse vertical resolution of the ERAI reanalysis dataset used in this study. For the sake of consistency, the ERAI results (together with the ERA5, MERRA2 and JRA3Q results) shown in Fig. 5 use the same dynamical quantities used to compute the $A_y$ term (Fig. 4). As mentioned in Sect. 2.4, BRAM2 uses 37 levels in the vertical (and around 30 in the stratosphere). This reduced number of levels (compared to the original 60 levels of ERAI) results in less precise vertical gradients that ultimately impact the $EPFD_z$ computation. In addition, the amplitudes of the $EPFD_z$ anomalies increase with finer vertical resolution. BRAM2 shows the smallest amplitudes with the coarsest resolution (30 levels in the stratosphere), then MERRA2 and JRA3Q (36 and 38 levels in the stratosphere, respectively) show larger amplitudes, and ERA5 and SD-WACCM deliver the largest amplitudes with the finest vertical resolution (45 and 40 levels in the stratosphere, respectively). A coarser vertical resolution implies larger vertical separation ($dz$) in the computation of the vertical gradients. This implies smaller vertical gradients, which play a major role in the definition of the $EPFD_z$ (Eq. 6b). Despite the differences in their magnitudes, the positive $EPFD_z$ anomalies in January 2019 corresponds to the enhanced $A_y$ term for the same month in Fig. 4. As mentioned before, this correspondence occurs because the breaking of planetary waves is the main driver of the meridional residual transport (assuming steady state and small sub-grid processes).

https://doi.org/10.5194/egusphere-2026-3449
Preprint. Discussion started: 25 June 2026


In early 2021, all datasets show large positive $EPFD_z$ anomalies (reaching 3 standard deviations) that are among the largest in the record and are comparable to the anomalies in January 2019. These $EPFD_z$ anomalies indicate enhanced wave breaking, but they do not correspond to significant anomalies in the $A_y$ term, nor in $N_2O$ or ozone concentrations for the same period (and no other term of the $N_2O$ TEM budget presents significantly large anomalies in that period). The lack of anomalies in the $A_y$ term in early 2021 indicates that the enhanced $EPFD_z$ did not substantially strengthen the meridional residual advection. This unexpected result can be explained by the different QBO phases in early 2019 and early 2021. The QBO in early 2019 was characterized by descending westerlies (W-QBO) with easterly winds at 50 hPa (Fig. S9), which generated a poleward secondary circulation at that level over. We will expand on the impact of the QBO on the anomalies in the next section. On the other hand, in early 2021, the QBO was in a transition period, with weak westerly winds across the whole tropical stratosphere (Fig. S10), resulting in a weak secondary circulation in the lower stratosphere (because the winds of the QBO secondary circulation peak and the maximum of the westerlies/easterlies). The weak secondary circulation in early 2021, which is primarily meridional in the lower stratosphere, is then the main driver of the differences between the large tracer anomalies in early 2019 compared to the absence of tracer anomalies in early 2021. In the following, we will focus on the anomalies in early 2019, and we will investigate their meridional and vertical structure, in order to illustrate the particular stratospheric conditions related to the QBO phase that occurred in early 2019.

## 4 Meridional and vertical structure of transport anomalies in the late 2018/2019 boreal winter

In this Section, we discuss latitude-pressure distributions of the $N_2O$, $A_y$, and $EPFD_z$ anomalies for selected months of the late 2018/2019 boreal winter. For $N_2O$, we show February 2019 because the anomalies maximize in that month, and because February marks the end of boreal winter, when the cumulative impact of the BDC is the strongest. For $A_y$ and the $EPFD_z$, we show January 2019, because their anomalies are the largest in that month (see previous figures). For each dataset, we aim to explore the latitudinal and vertical patterns of the $N_2O$, $A_y$ and $EPFD_z$ anomalies shown before only at 50 hPa. Unlike the previous Section, the anomalies shown here are not normalised by the standard deviation (but are still detrended) in order to keep the original units of each quantity.

### 4.1 $N_2O$ anomalies in February 2019

In this Section, we show latitude-vertical distributions of the anomalies of the $N_2O$ concentrations over the NH for February 2019 (Fig. 6). In the mid-upper stratosphere (roughly between 25 and 10 hPa), the $N_2O$ anomalies become negative for large part of the NH, minimizing in the subtropics. All datasets agree in the magnitude and pattern of these negative $N_2O$ anomalies. Above 10 hPa, the $N_2O$ anomalies in the NH change again sign and become slightly positive, but their magnitude and their meridional extension are largely reduced compared to the levels below. Over the Tropical region, all datasets show positive $N_2O$ anomalies above approximately 20 hPa. These positive anomalies are due to the upwelling from the lower levels that brings $N_2O$-rich air to the upper stratosphere (M2020).

https://doi.org/10.5194/egusphere-2026-3449
Preprint. Discussion started: 25 June 2026


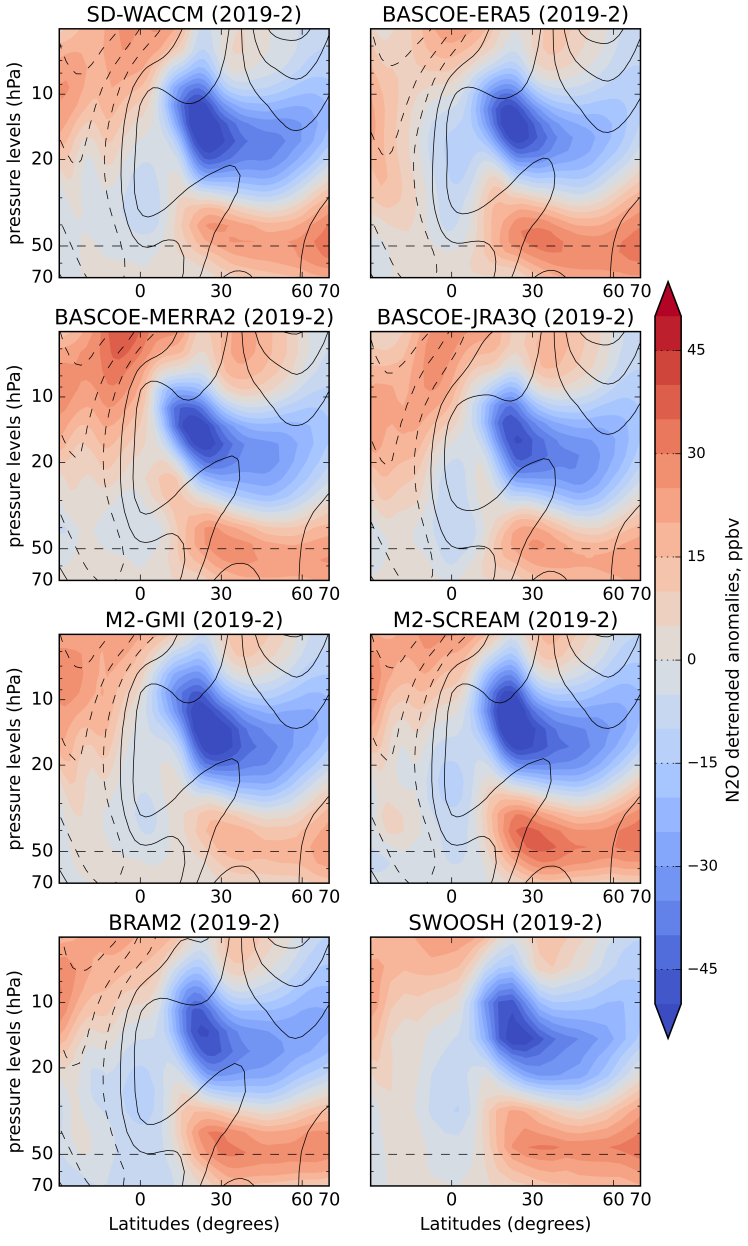


**Figure 6.** Latitude-Pressure cross sections of $N_2O$ anomalies (with respect to their climatology) for February 2019 for the NH. The linear trend has been removed from these anomalies. First row: SD-WACCM (left) and BASCOE-ERA5 (right). Second row: BASCOE-MERRA2 (left) and BASCOE-JRA3Q (right). Third row: M2-GMI (left) and M2-SCREAM (right). Fourth row: BRAM2 (left) and SWOOSH (right).

https://doi.org/10.5194/egusphere-2026-3449
Preprint. Discussion started: 25 June 2026


In the lower stratosphere below 30 hPa and equatorward of 15°N, Figure 6 shows near-zero or slightly negative $N_2O$ anomalies, and positive $N_2O$ anomalies between 15°N and 65-70°N. Equatorward of 15°N, all datasets broadly agree, with BRAM2 and M2-SCREAM slightly overestimating the amplitude of the weak negative $N_2O$ anomalies compared to SWOOSH. In the tropical lower stratosphere, $N_2O$ concentrations from Aura MLS show larger amplitudes in their seasonal cycle compared to ACE-FTS (Livesey et al., 2021). This discrepancy likely plays a role in the differences between BRAM2 and M2-SCREAM (only MLS-based) and SWOOSH (based on MLS and ACE-FTS) in the tropical lower stratosphere. Between 15°N and 65-70°N, all datasets show very similar $N_2O$ positive anomalies, with M2-GMI showing the smallest magnitude. In particular, the $N_2O$ positive anomaly at mid-latitudes at 50 hPa (see Fig. 2) is clearly visible in all datasets. The differences between M2-SCREAM and BRAM2 are minimal: the magnitudes and the patterns of the $N_2O$ anomalies are very similar between the two chemical reanalyses. This indicates that the assimilation of the MLS profiles successfully constrains the $N_2O$ concentrations at these latitudes, regardless of the driving meteorological reanalysis. Regarding the CTM experiments, the patterns of the $N_2O$ anomalies are broadly in agreement with the chemical reanalyses and SWOOSH. This indicates the consistency among the driving meteorological reanalyses in reproducing the latitudinal and vertical extent of the $N_2O$ anomaly. SD-WACCM shows results very similar to the CTM simulations, the chemical reanalyses and SWOOSH, indicating that its transport of $N_2O$ in February 2019 is realistic. In this study, the MERRA2 reanalysis is used to drive the BASCOE-MERRA2 simulation and M2-SCREAM, in a replay mode for M2-GMI, and as nudging dataset for SD-WACCM. All these methods deliver similar results for the $N_2O$ anomalies, but with some differences (e.g., different magnitude of the $N_2O$ anomalies in the northern mid-latitudes in the lower stratosphere). These small differences (of the order of few ppbvs) in the $N_2O$ concentrations indicate that changes in the treatment of the same meteorological quantities do not significantly alter the pattern of the $N_2O$ anomalies for such extreme events. This pattern of alternating signs and of such magnitudes in the $N_2O$ anomalies over the NH mid-latitudes is unique in our study and is not present at the end of previous boreal winters (see Figs. S11-S13).

Strahan et al. (2015) has showed that $N_2O$ anomalies generated by the QBO can propagate to the Antarctic in the SH. They demonstrated that QBO-induced $N_2O$ anomalies generated in the subtropics move towards the southern mid-latitudes and end up within the Antarctic polar vortex in the lower stratosphere. This QBO-induced transport process to the Antarctic takes approximately 1 year. Nevison et al. (2024) showed that the QBO signal can even impact the surface $N_2O$ growth rate in the SH with a time lag of 18 months. In the NH, the wave activity is significantly stronger than that over the SH because of the larger land-sea contrast. The larger wave activity increases the strength and variability of the stratospheric transport in the NH compared to the SH (Baldwin et al., 2021). Because of this stronger variability in the NH, QBO signals in the $N_2O$ concentrations (related to the secondary circulation induced by the QBO) are weaker in the NH compared to the SH (Strahan et al., 2015; Nevison et al., 2024). Nevertheless, we suggest that the $N_2O$ anomalies in February 2019 in Fig. 6 are caused by a combination of different dynamical and transport processes that involve the QBO, but with a much shorter time lag compared to the events described above. As mentioned before, within the Tropics and subtropics, the QBO induces the secondary circulation that depends on its phase (Strahan et al., 2015). In February 2019, the QBO was in a descending W-QBO phase with the zero wind line at 50 hPa. In the Tropics and subtropics, this QBO phase determines a secondary circulation that consists in enhanced poleward motion in the lower stratosphere and equatorward motion in the upper stratosphere. Such

https://doi.org/10.5194/egusphere-2026-3449
Preprint. Discussion started: 25 June 2026


secondary circulation usually generates negative $N_2O$ anomalies at the Equator and positive $N_2O$ anomalies in the subtropics in the lower stratosphere, and vice-versa in the upper stratosphere. In February 2019, the $N_2O$ anomalies slightly resemble the description above, but they peak around 30°N and extend into the mid-latitudes, and this extension is not visible in the pattern of the $N_2O$ anomalies with similar QBO conditions (Figs. S14-S16). In particular, the positive $N_2O$ anomalies at 50 hPa in February 2019 are much larger compared to previous similar QBO conditions. This indicates that the secondary circulation plays a role in determining the $N_2O$ anomalies, but also other transport and dynamical mechanism (related to the QBO) influence the stratospheric $N_2O$ anomalies in February 2019, especially in the extratropics. In the following, we will elucidate on the role of the secondary circulation and of other QBO-related dynamical processes in creating the $N_2O$ anomalies. The impact of the QBO (and its secondary circulation) in the northern extratropics (i.e., 30°-70°N) is not instantaneous, but it occurs with some time lag (Strahan et al., 2015). Given the shorter time lag in the NH compared to the SH, and given the results of the $A_y$ term shown before, in the next Section we will focus on the term that determines the $N_2O$ anomalies in February 2019, i.e., the $A_y$ term in January 2019.

### 4.2 Anomalies of the $A_y$ term in January 2019

In this Section, we show latitude-vertical distributions of the detrended anomalies of the $A_y$ term of the $N_2O$ TEM budget in the NH for January 2019 (Fig. 7). We will compare the $A_y$ anomalies with the $N_2O$ anomalies shown in Fig. 6. We highlight that the $A_y$ term is a tendency and contributes to the instantaneous and local rate of change of $N_2O$ (Abalos et al., 2013, M2020), while $N_2O$ is a cumulative quantity that continuously builds up in the atmosphere (Tian et al., 2020). Because of this fundamental difference, we limit our comparison to a qualitative analysis of the agreement of the signs of the $A_y$ and $N_2O$ anomalies, rather than a quantitative comparison of their magnitudes.

Above the Equator, the $A_y$ anomalies are generally small below 20 hPa. These small values are not surprising as the climatological $A_y$ term itself is small below 15 hPa during boreal winter (M2020). Above 20 hPa, all datasets show slightly positive $A_y$ anomalies. At these altitudes, the climatological $A_y$ term is approximately zero as this is the transition region between the two hemispheres, with almost zero or slightly negative values in the SH and positive values in the NH, indicating poleward advection of $N_2O$ in both hemispheres (M2020). The positive $A_y$ anomalies indicate then that the meridional advection is enhanced over that region, ultimately leading to positive $N_2O$ anomalies (see Fig. 6).

Over the subtropics, the $A_y$ anomalies are very small below 30/40 hPa. Above 20/30 hPa, the $A_y$ anomalies become largely negative, and extend further down to 60/70 hPa in BRAM2 and BASCOE-JRA3Q compared to the other datasets. BASCOE-JRA3Q also shows smaller magnitudes of the $A_y$ anomalies at these latitudes compared to the other CTM simulations. SD-WACCM successfully simulates the pattern of the $A_y$ anomalies but with reduced magnitude compared to the chemical reanalyses. In this subtropical region, the climatological $A_y$ term is positive in boreal winter (because of the northward residual advection) but with small magnitudes (M2020). As mentioned before, the QBO In January 2019 is in the descending W-QBO phase, and the secondary circulation in the subtropics is equatorward at the height of maximum westerlies (between 10 and 30 hPa) and poleward at the height of maximum easterlies (50 hPa). The negative $A_y$ anomalies between 10 and 20 hPa indicate then a weakening of the climatological northward advection that originates from the upper branch of the secondary circulation

https://doi.org/10.5194/egusphere-2026-3449
Preprint. Discussion started: 25 June 2026


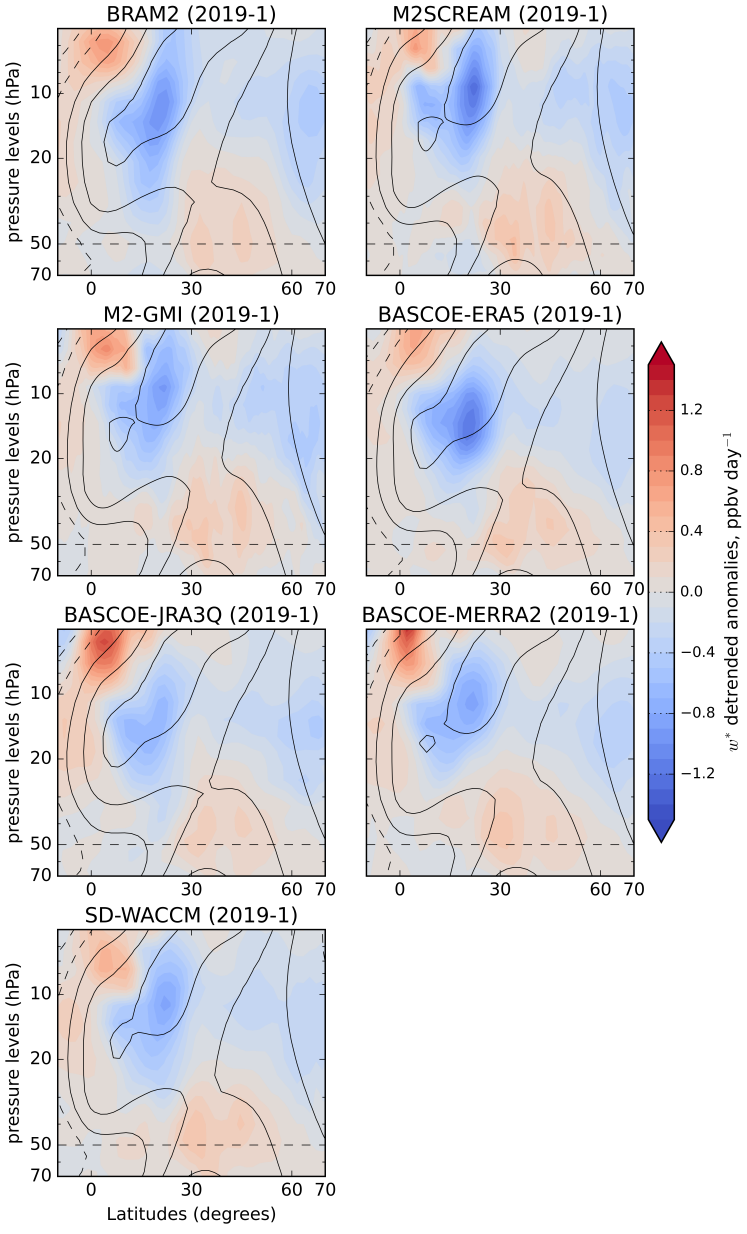


**Figure 7.** As Fig. 6, but for $A_y$ in January 2019.

https://doi.org/10.5194/egusphere-2026-3449
Preprint. Discussion started: 25 June 2026


directed equatorward. Such negative $A_y$ anomalies ultimately result in the negative $N_2O$ anomalies in February 2019 shown in Fig. 6. Around 40/50 hPa, the stronger poleward advection generated by the lower branch of the secondary circulation is visible in almost all the datasets as a slightly positive $A_y$ anomaly around 20°N. This slightly positive anomaly is not present in BRAM2 and BASCOE-JRA3Q. This indicates that the ERAI and JRA3Q dynamical reanalyses underestimate the strength of the lower branch of the secondary circulation pattern, at least in January 2019. The weaker secondary meridional advection in ERAI compared to ERA5 is consistent with the results of Diallo et al. (2021), who found that the QBO modulation of the BDC is stronger in ERA5 compared to ERAI above 20 km (approximately 60 hPa).

Over the mid-latitudes, all datasets show a consistent vertical dipole pattern of the $A_y$ anomalies, with positive values below 20 hPa and negative values above. In this latitudinal region, the climatological $A_y$ term is generally positive, indicating northward advection of $N_2O$ concentrations (M2020). Hence, the the structure of the $A_y$ anomalies indicates enhanced northward residual advection of $N_2O$ below 20 hPa, and weakened northward residual advection of $N_2O$ above 20 hPa. This pattern in the sign of the $A_y$ anomalies is similar to that of the $N_2O$ anomalies (Fig. 6), suggesting a causal relationship between the $A_y$ and the $N_2O$ anomalies. Around 50 hPa, the meridional component of the secondary circulation does not generally reach these latitudes, as it is usually confined in the subtropics where it is poleward in the lower stratosphere during descending W-QBO (Strahan et al., 2015). In the next Sections, we will elucidate the mechanism driving these $A_y$ anomalies (that determine the $N_2O$ anomalies) in the NH mid-latitudes.

Around 60-70°N, all datasets show negative $A_y$ anomalies in the whole stratosphere, with very similar magnitudes. The only exception is SD-WACCM that simulates smaller magnitudes compared to the other datasets. In this region, the climatological $A_y$ term has near-zero values, as the downwelling is the main driver of transport-driven $N_2O$ changes (M2020).

### 4.3 Anomalies of $EPFD_z$ in January 2019

Figure 8 is similar to Fig. 7 but for $EPFD_z$. We show anomalies of $EPFD_z$ because, as mentioned above, it dominates the EPFD anomalies in January 2019 compared to anomalies in $EPFD_y$. The EPFD (and specifically its vertical component $EPFD_z$) and their anomalies quantify the forcing from the breaking of the planetary waves, and are one of the main drivers of the residual circulation, hence also for its meridional component (Butchart, 2014; Baikhadzhaev et al., 2025). In general, negative values of $EPFD_z$ (related to convergence of the EP flux) indicate enhanced wave forcing, while positive $EPFD_z$ values (related to divergence of the EP flux) indicate inhibited wave forcing (Park et al., 2024). Contrarily to Fig. 5, we show the original $EPFD_z$ (i.e., without changing its sign). This way, negative $EPFD_z$ values represent enhanced forcing from the wave breaking and positive $EPFD_z$ indicate weakened forcing from the wave breaking. The goal of this Section is studying the meridional and vertical structure of the $EPFD_z$ anomalies in January 2019 in order to relate them to the $A_y$ anomalies in Fig. 7, and ultimately to the $N_2O$ anomalies (Fig. 6).

In the mid-upper stratosphere (between 10 and 20 hPa) in the mid-latitudes, the $EPFD_z$ anomalies are positive, indicating divergence of the vertical component of the EP flux, thus reduced planetary wave breaking. This pattern is consistent across the reanalyses and SD-WACCM. Concerning the ECMWF reanalyses, Diallo et al. (2021) showed that the planetary wave breaking is stronger in ERA5 than in ERAI in the extratropics between 30-40 km (2-13 hPa). This is not clearly visible in Fig.

https://doi.org/10.5194/egusphere-2026-3449
Preprint. Discussion started: 25 June 2026


8 as we consider a specific and short period. At these levels (2-13 hPa), the impact of the QBO easterlies at 50 hPa on the wave breaking is reduced compared to the lower stratosphere (Lu et al., 2020). On the other hand, the coupling between the phases of the QBO and of the Semi Annual Oscillation (SAO, Smith et al., 2017) could play a role in determining the planetary wave forcing, but this interaction is still a subject of research (Gray et al., 2022; Smith et al., 2023). The reduced wave breaking in the upper stratospheric mid-latitudes in January 2019 implies a reduced forcing for the residual circulation, which at these latitudes and altitudes consists mostly in the meridional poleward residual advection (Rosenlof, 1995; Butchart, 2014). As a result, the meridional residual advection is weakened in this region, and this is clear from the negative anomalies of $A_y$ term in the same region (Fig. 7). This reduction in the strength of the $A_y$ term ultimately leads to a reduction of the build-up of $N_2O$ for February 2019, which results in negative $N_2O$ anomalies (Fig. 6).

In the low stratosphere (below 20-30 hPa), all datasets agree in reproducing the negative $EPFD_z$ anomalies (i.e., enhanced wave forcing) at mid-latitudes. Such anomalies drive the anomalies in $A_y$ in the same region, which in turn determine the $N_2O$ anomalies one month later. Concerning the ECMWF reanalyses, the $EPFD_z$ anomalies are more positive (i.e., less negative) in ERA5 compared to ERAI, indicating reduced planetary wave breaking in ERA5 compared to ERAI. This is broadly consistent with Diallo et al. (2021), who showed that the climatological gravity wave breaking at the equatorial flank of the subtropical jet is weaker in ERA5 compared to ERAI. Recently, Kobayashi and Iwasaki (2024) showed that the climatological wave breaking is stronger in JRA3Q compared to ERA5 in the lower stratospheric (70-100 hPa) NH extra-tropics in DJF. This cannot be clearly seen in January 2019 (Fig. 8), as the $EPFD_z$ anomalies around 70 hPa are very similar between ERA5 and JRA3Q. In the next Section, we will investigate the causes of the anomalies in $EPFD_z$ (and $A_y$), and we will relate them to the secondary circulation and the Holton-Tan effect.

Poleward of 60°N, the $EPFD_z$ anomalies are negative across most of the stratosphere, indicating enhanced forcing from the wave breaking. Such enhanced forcing is related to the major Sudden Stratospheric Warming (SSW, Butler et al., 2017) that occurred in January 2019 (Lee and Butler, 2020). Such SSW in January 2019 was a split-type SSW and was conditioned by the QBO easterlies at 50 hPa (Lee and Butler, 2020; Butler et al., 2020). Despite the magnitude of the $EPFD_z$ anomalies, we do not discuss them in detail because they do not correspond to outstanding anomalies in $N_2O$ concentrations.

## 5 Dynamical causes of the anomalies in $EPFD_z$ and $A_y$

This Section aims to investigate the dynamical causes of the anomalies in $EPFD_z$ and $A_y$ that ultimately led to the anomalies in $N_2O$ concentrations. Given the prominent role of the QBO and of the secondary circulation in driving the anomalies, we will focus on the zonal ($u$) and meridional ($v$) components of the horizontal wind. As mentioned before, the QBO in January is in a W-QBO descending phase, and the zonal winds at 50 hPa are easterly. With these zonal wind conditions at 50 hPa, the Holton-Tan effect consists in more disturbed polar vortex, while the polar vortex is stronger and more stable with westerly winds at 50 hPa. Such relationship has been thoroughly studied both with models and satellite observations (Flury et al., 2013; Elsbury et al., 2021). In January 2019, given the easterly winds at 50 hPa, the Holton-Tan effect induces a strengthening of the planetary wave breaking in the mid-latitudes around 50 hPa (i.e., the negative $EPFD_z$ anomalies in Fig. 8) in all datasets,

https://doi.org/10.5194/egusphere-2026-3449
Preprint. Discussion started: 25 June 2026


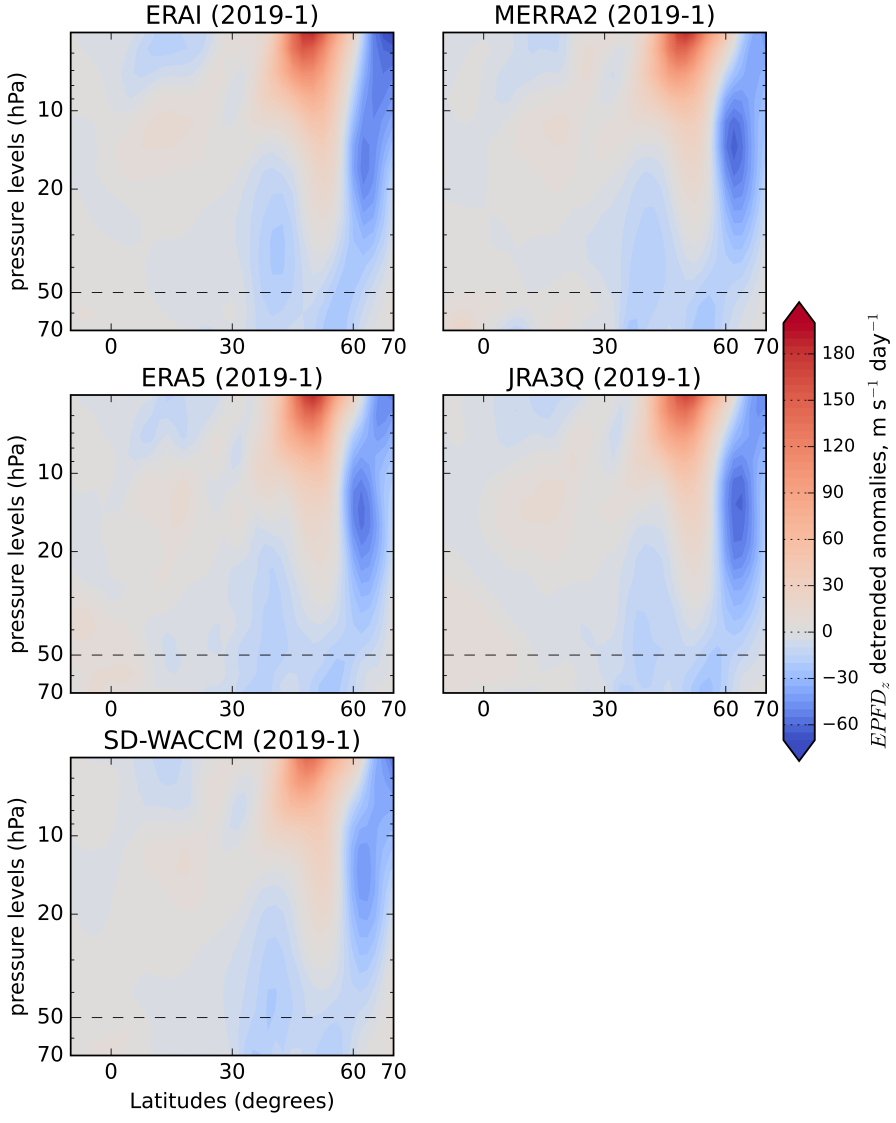


**Figure 8.** As Fig. 6, but for $EPFD_z$ in January 2019.

https://doi.org/10.5194/egusphere-2026-3449
Preprint. Discussion started: 25 June 2026


which in turn strengthens the meridional residual transport at 50 hPa (see Fig. 7). These results are consistent with those of Flury et al. (2013) in the lower stratosphere, where they find faster meridional transport during descending W-QBO phase. As mentioned before, one of the contributions to the Holton-Tan effect (i.e., the strengthened planetary wave forcing $EPFD_z$) in January 2019 arises from a northward shift of the QBO zero zonal wind line. As mentioned before, the QBO zero zonal wind line acts as a waveguide for planetary waves by modulating the occurrence of low-latitude wave breaking (Hitchman and Huesmann, 2009). With easterlies at 50 hPa, the zero zonal wind line generally shifts towards the winter subtropics, keeping the planetary waves forcing at higher latitudes (Anstey et al., 2022).

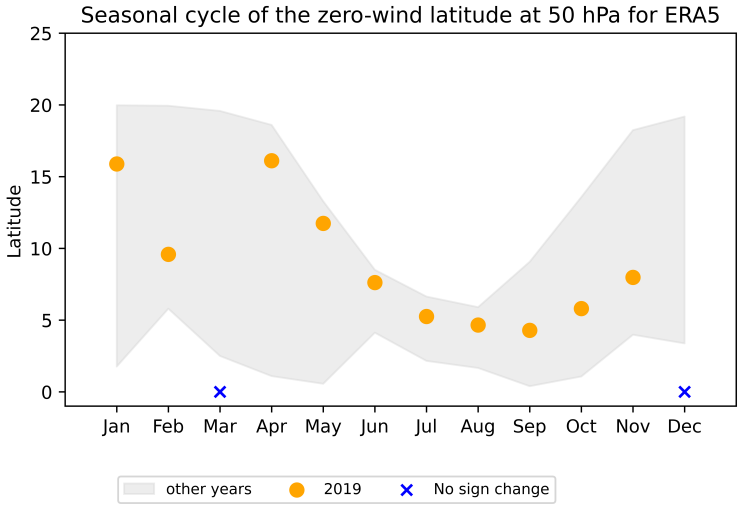


**Figure 9.** Annual cycle of the zero wind latitude at 50 hPa between 0°and 20°N for ERA5. The red dots indicate year 2019 and the shading indicates the minimum and maximum over the rest of the period. The blue crosses indicate months when the was no sign change of the zonal wind.

Figure 9 shows the seasonal cycle of the latitude of zero zonal wind line between 0°and 20°N at 50 hPa for ERA5. The zero zonal wind line shows a marked seasonal cycle, with the largest northward shift during boreal winter and the smallest during boreal summer. In January 2019, the northward shift of the zero zonal wind line was among the largest, but not the largest, with a northward displacement that reached 15°N. Such northward shift of the zero zonal wind line drove the negative anomalies in the $EPFD_z$ in January 2019 at 50 hPa in the mid-latitudes (the Holton-Tan effect, see Fig. 8), and contributed to the enhanced residual meridional advection at the same level (Fig. 7). The other reanalyses and SD-WACCM deliver very similar results (Figs. S17-S20).

The northward shift of the zero zonal wind line alone cannot explain the record-breaking anomalies of the $A_y$ term that occurred in January 2019. As mentioned before, the other contribution to the anomalous $A_y$ in January 2019 arises from the secondary circulation. During descending W-QBO phases, the secondary circulation in the subtropical lower stratosphere is directed poleward, and the easterlies at 50 hPa phase acts to re-inforce it at that level (Lu et al., 2020). Figure 10 shows

https://doi.org/10.5194/egusphere-2026-3449
Preprint. Discussion started: 25 June 2026


anomalies of the meridional wind $v$ (that contributes to the secondary circulation) in January as a function of latitude at 50 hPa for ERA5. We show the meridional wind $v$ because it comes into play in the calculation of $v^*$ (M2020), which is directly proportional to $A_y$. Over the northern subtropics (from the Equator to around 40°N), the anomalies of the meridional wind in 2019 are positive, indicating a northward motion that is consistent with the secondary circulation typical of the descending W-QBO phases. In addition, from the Equator to around 20°N, the anomalous meridional wind was stronger in January 2019 compared to the averages across the rest of the ERA5 record. From 20°N to around 35°N, the meridional wind anomalies in January 2019 are the largest of the ERA5 record, indicating the strongest poleward secondary circulation at 50 hPa in the record. Such large anomalies between 20°N and 35°N in the meridional wind are present also in the other reanalyses and SD-WACCM (Figs. S21-S24).

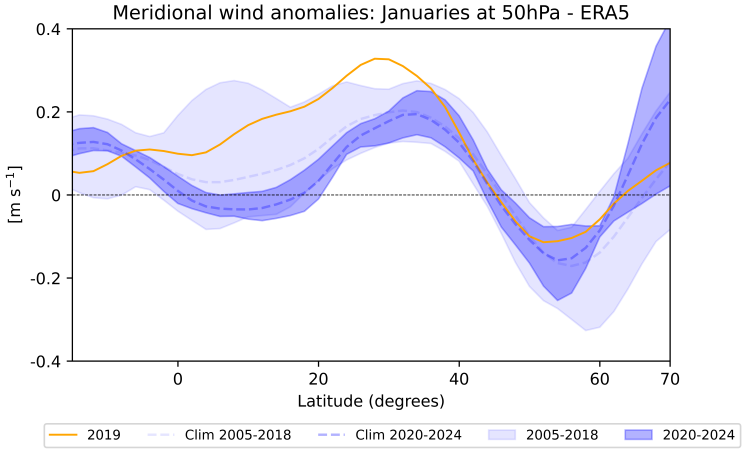


**Figure 10.** Latitudinal profiles of the anomalies of the meridional component of the wind $v$ [m/s] at 50 hPa for ERA5. The red line indicates January 2019. The light dashed blue line indicates the $v$ anomalies for the Januaries between 2005 and 2018. The dark dashed blue line indicates the $v$ anomalies for the Januaries between 2020 and 2024. The shadings indicate the minimum/maximum values of $v$ for the two periods mentioned above.

For January 2019, we suggest that the record-breaking poleward meridional residual advection in the lower stratospheric mid-latitudes arise from the combined effect of the two processes described in this Section. On one hand, the northward shift of the zero zonal wind line (the Holton-Tan effect) triggered enhanced wave breaking over the mid-latitudes, which in turn reinforced the eddies component of the meridional residual circulation. On the other hand, the anomalously strong poleward secondary circulation in the subtropics also resulted in a record-breaking meridional wind anomalies over the lower stratospheric subtropics and mid-latitudes. The combination of the anomalies of both the eddies and the meridional wind components resulted in the unprecedented enhancement of the meridional residual advection over the subtropics and mid-latitudes, which ultimately led to the transport of anomalously large $N_2O$ concentrations from the tropical region towards the northern mid-latitudes.

https://doi.org/10.5194/egusphere-2026-3449
Preprint. Discussion started: 25 June 2026


## 6 Summary and Conclusions

In this study, we investigated the exceptional anomalies in the $N_2O$ concentrations in the stratosphere in the NH in the late 2018/2019 boreal winter. To this end, we analyzed the impact of the meridional residual advection on the $N_2O$ concentrations (through the $N_2O$ TEM budget), and we related it to the forcing from the breaking of planetary waves (i.e., the EPFD and its vertical component). We further investigated the dynamical causes of these anomalies using the zonal and meridional components of the horizontal wind. We examined several datasets: the BASCOE CTM driven by three dynamical reanalyses (ERA5, JRA3Q and MERRA2), M2-GMI, the BRAM2 and M2-SCREAM chemical reanalyses, the SD-WACCM model (with the dynamics nudged towards MERRA2), and the SWOOSH merged observational dataset. This is the first intercomparison of this numbers of reanalyses for studies of stratospheric transport using $N_2O$ concentrations.

Across all datasets, the largely positive $N_2O$ anomaly in February 2019 stands out as the most striking transport-driven $N_2O$ perturbation in recent decades. The datasets agree very closely among each other, indicating that the $N_2O$ anomaly reveals an actual anomaly in stratospheric transport. In particular, the dynamical reanalyses driving the BASCOE CTM tend to show very similar results to the chemical reanalyses and SWOOSH. This is in agreement with previous studies using $N_2O$ and its TEM budget (M2020, M2022) and indicates that these dynamical reanalyses are still a powerful tool to study stratospheric transport, even for transport-driven extreme events. Concerning the $N_2O$ anomalies, the BASCOE-ERA5 simulation agrees best with the chemical reanalyses and with SWOOSH. This indicates that ERA5 simulates a more realistic stratospheric transport compared to JRA3Q and MERRA2. This difference is consistent with the more realistic $N_2O$ inter-annual variability in ERA5 compared to JRA55 and MERRA2 (M2022). The chemical reanalyses deliver very similar results to SWOOSH concerning the $N_2O$ and ozone anomalies, and their $N_2O$ TEM budget is consistent with the other datasets. The validity of the chemical reanalyses in detecting extreme events in stratospheric transport also paves the way to using them for extreme events related to chemical processes (e.g., wildfires, extreme polar vortex conditions), especially because of their regular temporal and spatial coverage. The results from SD-WACCM agree well with those of the chemical reanalyses and SWOOSH. This is in line with Chrysanthou et al. (2019), who showed that nudged dynamics delivers more realistic inter-annual variability in chemistry climate models compared to their free-running versions.

The TEM diagnostics indicates that the $N_2O$ anomalies in the NH in February 2019 originate from enhanced meridional residual advection in January 2019, which is in turn partly generated by enhanced planetary wave activity over the same region and period. The enhanced planetary wave activity anomaly was generated by one of the largest northward shifts of the zero-wind line in the dataset records, reaching around 15°N. In addition, the descending W-QBO phase (corresponding to easterlies at 50 hPa) in January 2019 generated a anomalously strong secondary circulation that was directed poleward in the NH at the level of maximum easterlies. The combination of the exceptionally strong poleward secondary circulation with the enhanced planetary wave activity generated the extreme residual meridional advection in January 2019, and in turn the positive $N_2O$ anomalies in the lower stratosphere in February 2019. This combination of processes highlights the importance of the secondary circulation in combination with an enhanced (or reduced) planetary wave activity due to the Holton-Tan effect in creating these $N_2O$ anomalies. In particular, we emphasize the importance of considering the QBO secondary circulation when

https://doi.org/10.5194/egusphere-2026-3449
Preprint. Discussion started: 25 June 2026


studying transport-related processes in the extratropical mid-lower stratosphere. Under the specific circumstances described in this work, the meridional residual advection can extend to the edge of the polar vortex, and may impact polar processes via the transport of constituents relevant for ozone chemistry (e.g., HCl). Moreover, a better understanding of the extratropical role and extent of the secondary circulation can shed some light on the large uncertainties on the ozone trends in the northern mid-latitudes (Benito-Barca et al., 2025), a region that can be substantially impacted by an extended secondary circulation. In future climate projection under warming conditions, the zero zonal wind line is projected to be displaced both vertically and meridionally (Kawatani et al., 2011). In addition, the secondary meridional circulation is projected to become stronger in late winter in the NH under a warming climate (Karami et al., 2023). Given these QBO-related perturbations with climate change, especially the strengthening of the secondary circulation in the NH, we argue that the episode of late 2018/2019 boreal winter can be one of the early episodes of enhanced secondary circulation in the observational record.

$N_2O$ has been shown to be a valuable tracer to study trends in the stratospheric circulation (e.g., Dubé et al., 2023, M2022). The present study shows that $N_2O$ concentrations can be used as a diagnostics also for other dynamically-driven extreme events in the stratosphere. Such dynamically-driven extreme events are not limited to QBO-related processes, but can arise from a variety of sources: large volcanic eruptions that reach the stratosphere (e.g., the Hunga eruption, Wilmouth et al., 2023) or large wildfires that significantly change the temperature of the lower stratosphere (Stocker et al., 2021). In particular, since wildfires are likely to become more frequent and intense with a changing climate (Jones et al., 2022), temperature changes related to wildfires are likely to become more pronounced and reach the stratosphere (e.g., the Australian 2019/2020 wildfires, Yu et al., 2021). Temperature changes impact zonal winds through thermal wind balance and can alter the residual circulation by modifying the eddy heat fluxes that contribute to it. Hence, we expect that $N_2O$ will be further impacted by such possible perturbations in the stratospheric transport, and the analysis of the $N_2O$ changes will lead to a better understanding of the evolution of stratospheric transport under such extreme events.

Finally, the continuity of global $N_2O$ measurements is an important concern, as key satellites such as MLS and ACE-FTS are reaching the end of their operational lifetimes, and there is no confirmed plan to extend daily satellite $N_2O$ measurements (Salawitch et al., 2025). Other current (and upcoming) satellite missions can provide profiles of stratospheric tracers, but their tracer coverage is limited compared to MLS and ACE-FTS: for example, the upcoming Atmospheric Limb Tracker for the Investigation of the Upcoming Stratosphere (ALTIUS, Fussen et al., 2019) will measure profiles of $CH_4$, water vapor, ozone and possibly $SF_6$, and the Ozone Mapping and Profiler Suite Limb Profiler (OMPS-LP, Kramarova et al., 2018) currently provides ozone measurements. Recently, the National Aeronautics and Space Administration selected the STRIVE (Stratosphere Troposphere Response using Infrared Vertically-resolved light Explorer) mission, marking an important step in extending stratospheric monitoring. STRIVE will measure emitted and scattered radiation profiles in the infrared to provide profiles of temperatures, trace gases concentrations, aerosols extinctions and cloud properties in the limb geometry in both day and night (Jaeglé et al., 2025). With its very fine vertical resolution and an unprecedented horizontal sampling, together with multi-species measurements beyond ozone (including $N_2O$), STRIVE will substantially contribute to atmospheric composition studies. However, its launch will not occur before 2030, leaving a multi-year gap when $N_2O$ measurement capabilities will remain limited. Ground-based measurement can help filling this gap (e.g., the Network for the Detection of Atmospheric Com-

https://doi.org/10.5194/egusphere-2026-3449
Preprint. Discussion started: 25 June 2026


position Changes, Petropavlovskikh et al., 2026), even though their intrinsic limitations (e.g., their sparseness over the tropical region) can reduce the potential scientific interpretations compared to satellite measurements. The extreme event analyzed in this study (and the likely increase of extreme events with a warming climate) highlight the importance of maintaining continuous observations of long-lived tracers to investigate dynamically-driven extremes and to monitor the changing stratosphere.

*Data availability.* The SWOOSH data can be accessed via https://csl.noaa.gov/groups/csl8/swoosh/. The M2-GMI data can be accessed via: https://portal.nccs.nasa.gov/datashare/merra2_gmi/. The M2-SCREAM data can be accessed via: https://disc.gsfc.nasa.gov/datasets?keywords=M2-SCREAM&page=1. The BRAM2 data can be accessed via: https://strato.aeronomie.be/?view=article&id=6:bram&catid=2:uncategorised. The $N_2O$ and ozone monthly zonal means concentrations, the monthly zonal mean zonal and meridional winds, the monthly $A_y$ term of the $N_2O$ budget and the monthly EPFD are freely available at: https://doi.org/10.18758/wfv3fdib (Minganti, 2026).

*Author contributions.* DM and KW had the idea of the study. DM carried out the analysis, computed the TEM budget, made the figures and wrote most of the manuscript. SC and KW contributed to the interpretation and discussion of the results since their earliest stage. KW provided the M2-SCREAM and M2-GMI datasets. SD provided the SWOOSH and SD-WACCM datasets. QE provided the BRAM2 chemical reanalysis. SV performed the BASCOE simulation and wrote the BASCOE CTM section. MO, CW, SD and ER contributed to the interpretation of the results. All authors revised the manuscript and provided feedback on the results and on the writing.

*Competing interests.* The authors declare that they have no conflict of interest

*Acknowledgements.* The authors acknowledge the financial support from the FED-tWIN programme of the Belgian Federal Science Policy Office (BELSPO) and the joint initiative of BIRA-IASB and ULB within the framework of the project [Prf-2021R-045]. Generative AI was used to partly produce the Python routine to handle the dat file format and to clarify specifc Python commands/functions.

https://doi.org/10.5194/egusphere-2026-3449
Preprint. Discussion started: 25 June 2026


## References

Abalos, M., Randel, W., Kinnison, D., and Serrano, E.: Quantifying tracer transport in the tropical lower stratosphere using WACCM, Atmospheric Chemistry and Physics, 13, 10 591–10 607, 2013.

Andrews, D. G., Holton, J. R., and Leovy, C. B.: Middle atmosphere dynamics, 40, Academic press, 1987.

Anstey, J. A. and Shepherd, T. G.: High-latitude influence of the quasi-biennial oscillation, Quarterly Journal of the Royal Meteorological Society, 140, 1–21, https://doi.org/https://doi.org/10.1002/qj.2132, 2014.

Anstey, J. A., Osprey, S. M., Alexander, J., Baldwin, M. P., Butchart, N., Gray, L., Kawatani, Y., Newman, P. A., and Richter, J. H.: Impacts, processes and projections of the quasi-biennial oscillation, Nature Reviews Earth & Environment, 3, 588–603, https://doi.org/https://doi.org/10.1038/s43017-022-00323-7, 2022.

Baikhadzhaev, R., Ploeger, F., Preusse, P., Ern, M., and Birner, T.: A dynamics-based separation of deep and shallow stratospheric circulation branches, Atmospheric Chemistry and Physics, 25, 12 753–12 777, https://doi.org/10.5194/acp-25-12753-2025, 2025.

Baldwin, M., Gray, L., Dunkerton, T., Hamilton, K., Haynes, P., Randel, W., Holton, J., Alexander, M., Hirota, I., Horinouchi, T., et al.: The quasi-biennial oscillation, Reviews of Geophysics, 39, 179–229, 2001.

Baldwin, M. P., Ayarzagüena, B., Birner, T., Butchart, N., Butler, A. H., Charlton-Perez, A. J., Domeisen, D. I. V., Garfinkel, C. I., Garny, H., Gerber, E. P., Hegglin, M. I., Langematz, U., and Pedatella, N. M.: Sudden Stratospheric Warmings, Reviews of Geophysics, 59, e2020RG000 708, https://doi.org/https://doi.org/10.1029/2020RG000708, 2021.

Ball, W. T., Alsing, J., Staehelin, J., Davis, S. M., Froidevaux, L., and Peter, T.: Stratospheric ozone trends for 1985–2018: sensitivity to recent large variability, Atmospheric Chemistry and Physics, 19, 12 731–12 748, 2019.

Benito-Barca, S., Abalos, M., Calvo, N., Garny, H., Birner, T., Abraham, N. L., Akiyoshi, H., Dennison, F., Jöckel, P., Josse, B., et al.: Recent lower stratospheric ozone trends in CCMI-2022 models: Role of natural variability and transport, Journal of Geophysical Research: Atmospheres, 130, e2024JD042 412, 2025.

Bernath, P.: The atmospheric chemistry experiment (ACE), Journal of Quantitative Spectroscopy and Radiative Transfer, 186, 3–16, 2017.

Birner, T. and Bönisch, H.: Residual circulation trajectories and transit times into the extratropical lowermost stratosphere, Atmospheric Chemistry and Physics, 11, 817–827, 2011.

Brasseur, G. P. and Solomon, S.: Aeronomy of the middle atmosphere: Chemistry and physics of the stratosphere and mesosphere, vol. 32, Springer Science & Business Media, 2005.

Brewer, A. W.: Evidence for a world circulation provided by the measurements of helium and water vapour distribution in the stratosphere, Quarterly Journal of the Royal Meteorological Society, 75, 351–363, https://doi.org/10.1002/qj.49707532603, 1949.

Butchart, N.: The Brewer-Dobson circulation, Reviews of Geophysics, 52, 157–184, https://doi.org/https://doi.org/10.1002/2013RG000448, 2014.

Butchart, N.: The stratosphere: A review of the dynamics and variability, Weather and Climate Dynamics, 3, 1237–1272, 2022.

Butler, A. H., Sjoberg, J. P., Seidel, D. J., and Rosenlof, K. H.: A sudden stratospheric warming compendium, Earth System Science Data, 9, 63–76, 2017.

Butler, A. H., Lawrence, Z. D., Lee, S. H., Lillo, S. P., and Long, C. S.: Differences between the 2018 and 2019 stratospheric polar vortex split events, Quarterly Journal of the Royal Meteorological Society, 146, 3503–3521, 2020.

https://doi.org/10.5194/egusphere-2026-3449
Preprint. Discussion started: 25 June 2026


Chabrillat, S., Vigouroux, C., Christophe, Y., Engel, A., Errera, Q., Minganti, D., Monge-Sanz, B. M., Segers, A., and Mahieu, E.: Comparison of mean age of air in five reanalyses using the BASCOE transport model, Atmospheric Chemistry and Physics, 18, 14 715–14 735, 2018.

Chabrillat, S., Rémy, S., Errera, Q., Huijnen, V., Bingen, C., Debosscher, J., Hendrick, F., Metzger, S., Mora, A., Minganti, D., et al.: Modelling stratospheric composition for the Copernicus Atmosphere Monitoring Service: multi-species evaluation of IFS-COMPO Cy49, Geoscientific Model Development, 18, 8973–9014, 2025.

Chipperfield, M. P., Dhomse, S., Hossaini, R., Feng, W., Santee, M. L., Weber, M., Burrows, J. P., Wild, J. D., Loyola, D., and Coldewey-Egbers, M.: On the cause of recent variations in lower stratospheric ozone, Geophysical Research Letters, 45, 5718–5726, 2018.

Choi, W., Lee, H., Grant, W. B., Park, J. H., Holton, J. R., Lee, K.-M., and Naujokat, B.: On the secondary meridional circulation associated with the quasi-biennial oscillation, Tellus B: Chemical and Physical Meteorology, 54, 395–406, 2002.

Chrysanthou, A., Maycock, A. C., Chipperfield, M. P., Dhomse, S., Garny, H., Kinnison, D., Akiyoshi, H., Deushi, M., Garcia, R. R., Jöckel, P., et al.: The effect of atmospheric nudging on the stratospheric residual circulation in chemistry–climate models, Atmospheric Chemistry and Physics, 19, 11 559–11 586, 2019.

Costa, M. H., Cotrim da Cunha, L., Cox, P. M., Eliseev, A. V., Hensen, S., Ishii, M., Jaccard, S., Koven, C., Lohila, A., Patra, P. K., et al.: Global carbon and other biogeochemical cycles and feedbacks, IPCC, 2021.

Crutzen, P. J.: The influence of nitrogen oxides on the atmospheric ozone content, Quarterly Journal of the Royal Meteorological Society, 96, 320–325, 1970.

Damian, V., Sandu, A., Damian, M., Potra, F., and Carmichael, G. R.: The kinetic preprocessor KPP-a software environment for solving chemical kinetics, Computers & Chemical Engineering, 26, 1567–1579, 2002.

Danabasoglu, G., Lamarque, J.-F., Bacmeister, J., Bailey, D., DuVivier, A., Edwards, J., Emmons, L., Fasullo, J., Garcia, R., Gettelman, A., et al.: The community earth system model version 2 (CESM2), Journal of Advances in Modeling Earth Systems, 12, 2020.

Davis, N. A., Callaghan, P., Simpson, I. R., and Tilmes, S.: Specified dynamics scheme impacts on wave-mean flow dynamics, convection, and tracer transport in CESM2 (WACCM6), Atmospheric Chemistry and Physics, 22, 197–214, https://doi.org/10.5194/acp-22-197-2022, 2022.

Davis, N. A., Visioni, D., Garcia, R. R., Kinnison, D. E., Marsh, D. R., Mills, M., Richter, J. H., Tilmes, S., Bardeen, C. G., Gettelman, A., Glanville, A. A., MacMartin, D. G., Smith, A. K., and Vitt, F.: Climate, Variability, and Climate Sensitivity of ̌201cMiddle Atmosphere̲201d Chemistry Configurations of the Community Earth System Model Version 2, Whole Atmosphere Community Climate Model Version 6 (CESM2(WACCM6)), Journal of Advances in Modeling Earth Systems, 15, e2022MS003 579, https://doi.org/https://doi.org/10.1029/2022MS003579, e2022MS003579 2022MS003579, 2023a.

Davis, S. M., Rosenlof, K. H., Hassler, B., Hurst, D. F., Read, W. G., Vömel, H., Selkirk, H., Fujiwara, M., and Damadeo, R.: The Stratospheric Water and Ozone Satellite Homogenized (SWOOSH) database: a long-term database for climate studies, Earth System Science Data, 8, 461–490, https://doi.org/10.5194/essd-8-461-2016, 2016.

Davis, S. M., Davis, N., Portmann, R. W., Ray, E., and Rosenlof, K.: The role of tropical upwelling in explaining discrepancies between recent modeled and observed lower-stratospheric ozone trends, Atmospheric Chemistry and Physics, 23, 3347–3361, https://doi.org/10.5194/acp-23-3347-2023, 2023b.

Dee, D. P., Uppala, S. M., Simmons, A. J., Berrisford, P., Poli, P., Kobayashi, S., Andrae, U., Balmaseda, M. A., Balsamo, G., Bauer, P., Bechtold, P., Beljaars, A. C. M., van de Berg, L., Bidlot, J., Bormann, N., Delsol, C., Dragani, R., Fuentes, M., Geer, A. J., Haimberger, L., Healy, S. B., Hersbach, H., Hólm, E. V., Isaksen, L., Kållberg, P., Köhler, M., Matricardi, M., McNally, A. P., Monge-Sanz,

https://doi.org/10.5194/egusphere-2026-3449
Preprint. Discussion started: 25 June 2026


B. M., Morcrette, J.-J., Park, B.-K., Peubey, C., de Rosnay, P., Tavolato, C., Thépaut, J.-N., and Vitart, F.: The ERA-Interim reanalysis: configuration and performance of the data assimilation system, Quarterly Journal of the Royal Meteorological Society, 137, 553–597, https://doi.org/https://doi.org/10.1002/qj.828, 2011.

Diallo, M., Ern, M., and Ploeger, F.: The advective Brewer–Dobson circulation in the ERA5 reanalysis: climatology, variability, and trends, Atmospheric Chemistry and Physics, 21, 7515–7544, 2021.

Dobson, G. M. B. and Massey, H. S. W.: Origin and distribution of the polyatomic molecules in the atmosphere, Proceedings of the Royal Society of London. Series A. Mathematical and Physical Sciences, 236, 187–193, https://doi.org/10.1098/rspa.1956.0127, 1956.

Douglass, A. R., Stolarski, R. S., Strahan, S. E., and Connell, P. S.: Radicals and reservoirs in the GMI chemistry and transport model: Comparison to measurements, Journal of Geophysical Research: Atmospheres, 109, 2004.

Dubé, K., Tegtmeier, S., Bourassa, A., Zawada, D., Degenstein, D., Sheese, P. E., Walker, K. A., and Randel, W.: N 2 O as a regression proxy for dynamical variability in stratospheric trace gas trends, Atmospheric Chemistry and Physics, 23, 13 283–13 300, 2023.

Duncan, B. N., Logan, J., Bey, I., Megretskaia, I., Yantosca, R., Novelli, P. C., Jones, N. B., and Rinsland, C.: Global budget of CO, 1988–1997: Source estimates and validation with a global model, Journal of Geophysical Research: Atmospheres, 112, 2007.

Edmon Jr, H., Hoskins, B., and McIntyre, M.: Eliassen-Palm cross sections for the troposphere, Journal of the Atmospheric Sciences, 37, 2600–2616, 1980.

Elsbury, D., Peings, Y., and Magnusdottir, G.: CMIP6 models underestimate the Holton-Tan effect, Geophysical Research Letters, 48, e2021GL094 083, 2021.

Errera, Q., Daerden, F., Chabrillat, S., Lambert, J., Lahoz, W., Viscardy, S., Bonjean, S., and Fonteyn, D.: 4D-Var assimilation of MIPAS chemical observations: ozone and nitrogen dioxide analyses, Atmospheric Chemistry and Physics, 8, 6169–6187, 2008.

Errera, Q., Chabrillat, S., Christophe, Y., Debosscher, J., Hubert, D., Lahoz, W., Santee, M. L., Shiotani, M., Skachko, S., von Clarmann, T., and Walker, K.: Technical note: Reanalysis of Aura MLS chemical observations, Atmospheric Chemistry and Physics, 19, 13 647–13 679, https://doi.org/10.5194/acp-19-13647-2019, 2019.

Fischer, H., Birk, M., Blom, C., Carli, B., Carlotti, M., Von Clarmann, T., Delbouille, L., Dudhia, A., Ehhalt, D., Endemann, M., et al.: MIPAS: an instrument for atmospheric and climate research, Atmospheric Chemistry and Physics, 8, 2151–2188, 2008.

Flury, T., Wu, D. L., and Read, W.: Variability in the speed of the Brewer–Dobson circulation as observed by Aura/MLS, Atmospheric Chemistry and Physics, 13, 4563–4575, 2013.

Froidevaux, L., Kinnison, D. E., Wang, R., Anderson, J., and Fuller, R. A.: Evaluation of CESM1 (WACCM) free-running and specified dynamics atmospheric composition simulations using global multispecies satellite data records, Atmospheric Chemistry and Physics, 19, 4783–4821, https://doi.org/10.5194/acp-19-4783-2019, 2019.

Fussen, D., Baker, N., Debosscher, J., Dekemper, E., Demoulin, P., Errera, Q., Franssens, G., Mateshvili, N., Pereira, N., Pieroux, D., et al.: The ALTIUS atmospheric limb sounder, Journal of Quantitative Spectroscopy and Radiative Transfer, 238, 106 542, 2019.

Garfinkel, C. I., Shaw, T. A., Hartmann, D. L., and Waugh, D. W.: Does the Holton–Tan mechanism explain how the quasi-biennial oscillation modulates the Arctic polar vortex?, Journal of the Atmospheric Sciences, 69, 1713–1733, 2012.

Garny, H., Birner, T., Bönisch, H., and Bunzel, F.: The effects of mixing on age of air, Journal of Geophysical Research: Atmospheres, 119, 7015–7034, 2014.

Garny, H., Ploeger, F., Abalos, M., Bönisch, H., Castillo, A. E., von Clarmann, T., Diallo, M., Engel, A., Laube, J. C., Linz, M., et al.: Age of stratospheric air: Progress on processes, observations, and long-term trends, Reviews of Geophysics, 62, e2023RG000 832, 2024.

https://doi.org/10.5194/egusphere-2026-3449
Preprint. Discussion started: 25 June 2026


Gelaro, R., McCarty, W., Suárez, M. J., Todling, R., Molod, A., Takacs, L., Randles, C. A., Darmenov, A., Bosilovich, M. G., Reichle, R., Wargan, K., Coy, L., Cullather, R., Draper, C., Akella, S., Buchard, V., Conaty, A., da Silva, A. M., Gu, W., Kim, G.-K., Koster, R., Lucchesi, R., Merkova, D., Nielsen, J. E., Partyka, G., Pawson, S., Putman, W., Rienecker, M., Schubert, S. D., Sienkiewicz, M., and Zhao, B.: The Modern-Era Retrospective Analysis for Research and Applications, Version 2 (MERRA-2), Journal of Climate, 30, 5419 – 5454, https://doi.org/10.1175/JCLI-D-16-0758.1, 2017.

Gettelman, A., Mills, M., Kinnison, D., Garcia, R., Smith, A., Marsh, D., Tilmes, S., Vitt, F., Bardeen, C., McInerny, J., et al.: The whole atmosphere community climate model version 6 (WACCM6), Journal of Geophysical Research: Atmospheres, 124, 12 380–12 403, 2019.

Gray, L. J., Anstey, J. A., Kawatani, Y., Lu, H., Osprey, S., and Schenzinger, V.: Surface impacts of the Quasi Biennial Oscillation, Atmospheric Chemistry and Physics, 18, 8227–8247, https://doi.org/10.5194/acp-18-8227-2018, 2018.

Gray, L. J., Lu, H., Brown, M. J., Knight, J. R., and Andrews, M. B.: Mechanisms of influence of the Semi-Annual Oscillation on stratospheric sudden warmings, Quarterly Journal of the Royal Meteorological Society, 148, 1223–1241, 2022.

Hegglin, M. I. and Shepherd, T. G.: O3-N2O correlations from the Atmospheric Chemistry Experiment: Revisiting a diagnostic of transport and chemistry in the stratosphere, Journal of Geophysical Research: Atmospheres, 112, https://doi.org/https://doi.org/10.1029/2006JD008281, 2007.

Hersbach, H., Bell, B., Berrisford, P., Hirahara, S., Horányi, A., Muñoz-Sabater, J., Nicolas, J., Peubey, C., Radu, R., Schepers, D., et al.: The ERA5 global reanalysis, Quarterly Journal of the Royal Meteorological Society, 146, 1999–2049, 2020.

Hitchcock, P. and Ming, A.: The Role of Ozone in the Secondary Circulation of the QBO: Linear Theory, Journal of Geophysical Research: Atmospheres, 130, e2025JD044 766, https://doi.org/https://doi.org/10.1029/2025JD044766, e2025JD044766 2025JD044766, 2025.

Hitchman, M. H. and Huesmann, A. S.: Seasonal influence of the quasi-biennial oscillation on stratospheric jets and Rossby wave breaking, Journal of the Atmospheric Sciences, 66, 935–946, 2009.

Holton, J.: An Introduction to Dynamic Meteorology, An Introduction to Dynamic Meteorology, Elsevier Academic Press, ISBN 9780123540157, https://books.google.it/books?id=fhW5oDv3EPsC, 2004.

Holton, J. R. and Tan, H.-C.: The influence of the equatorial quasi-biennial oscillation on the global circulation at 50 mb, Journal of Atmospheric Sciences, 37, 2200–2208, 1980.

Jaeglé, L., Wang, J., Oman, L., and DeLand, M.: The STRIVE Earth System Explorer Mission Concept, in: EGU General Assembly Conference Abstracts, pp. EGU25–7598, 2025.

Jones, M. W., Abatzoglou, J. T., Veraverbeke, S., Andela, N., Lasslop, G., Forkel, M., Smith, A. J., Burton, C., Betts, R. A., van der Werf, G. R., et al.: Global and regional trends and drivers of fire under climate change, Reviews of Geophysics, 60, e2020RG000 726, 2022.

Karami, K., Garcia, R., Jacobi, C., Richter, J. H., and Tilmes, S.: The Holton–Tan mechanism under stratospheric aerosol intervention, Atmospheric Chemistry and Physics, 23, 3799–3818, https://doi.org/10.5194/acp-23-3799-2023, 2023.

Kawatani, Y., Hamilton, K., and Watanabe, S.: The Quasi-Biennial Oscillation in a Double CO2 Climate, Journal of the Atmospheric Sciences, 68, 265 – 283, https://doi.org/10.1175/2010JAS3623.1, 2011.

Kidston, J., Scaife, A. A., Hardiman, S. C., Mitchell, D. M., Butchart, N., Baldwin, M. P., and Gray, L. J.: Stratospheric influence on tropospheric jet streams, storm tracks and surface weather, Nature Geoscience, 8, 433–440, 2015.

Kim, Y.-H.: Explaining the period fluctuation of the quasi-biennial oscillation, Atmospheric Chemistry and Physics, 25, 5647–5664, https://doi.org/10.5194/acp-25-5647-2025, 2025.

Kobayashi, C. and Iwasaki, T.: The Brewer-Dobson circulation in the JRA-3Q reanalysis and the impact of changes in model physical processes, Quarterly Journal of the Royal Meteorological Society, 150, 5605–5620, https://doi.org/https://doi.org/10.1002/qj.4896, 2024.

https://doi.org/10.5194/egusphere-2026-3449
Preprint. Discussion started: 25 June 2026


Kosaka, Y., Kobayashi, S., Harada, Y., Kobayashi, C., Naoe, H., Yoshimoto, K., Harada, M., Goto, N., Chiba, J., Miyaoka, K., et al.: The JRA-3Q reanalysis, Journal of the Meteorological Society of Japan. Ser. II, 102, 49–109, 2024.

Kramarova, N. A., Bhartia, P. K., Jaross, G., Moy, L., Xu, P., Chen, Z., DeLand, M., Froidevaux, L., Livesey, N., Degenstein, D., et al.: Validation of ozone profile retrievals derived from the OMPS LP version 2.5 algorithm against correlative satellite measurements, Atmospheric Measurement Techniques, 11, 2837–2861, 2018.

Kumar, V., Hitchman, M. H., Du, W., Dhaka, S., and Yoden, S.: Teleconnection of the Quasi-biennial oscillation with boreal winter surface climate in Eurasia and North America, Communications Earth & Environment, 5, 251, 2024.

Kuttippurath, J., Gopikrishnan, G. P., Müller, R., Godin-Beekmann, S., and Brioude, J.: No severe ozone depletion in the tropical stratosphere in recent decades, Atmospheric Chemistry and Physics, 24, 6743–6756, 2024.

Lee, S. H. and Butler, A. H.: The 2018-2019 Arctic stratospheric polar vortex, Weather, 75, 52–57, https://doi.org/https://doi.org/10.1002/wea.3643, 2020.

Levelt, P. F., Van Den Oord, G. H., Dobber, M. R., Malkki, A., Visser, H., De Vries, J., Stammes, P., Lundell, J. O., and Saari, H.: The ozone monitoring instrument, IEEE Transactions on geoscience and remote sensing, 44, 1093–1101, 2006.

Levelt, P. F., Joiner, J., Tamminen, J., Veefkind, J. P., Bhartia, P. K., Stein Zweers, D. C., Duncan, B. N., Streets, D. G., Eskes, H., van der A, R., et al.: The Ozone Monitoring Instrument: overview of 14 years in space, Atmospheric Chemistry and Physics, 18, 5699–5745, 2018.

Lin, S.-J. and Rood, R. B.: Multidimensional flux-form semi-Lagrangian transport schemes, Monthly Weather Review, 124, 2046–2070, 1996.

Livesey, N. J., Read, W. G., Froidevaux, L., Lambert, A., Santee, M. L., Schwartz, M. J., Millan, L. F., Jarnot, R. F., Wagner, P. A., Hurst, D. F., Walker, K. A., Sheese, P. E., and Nedoluha, G. E.: Investigation and amelioration of long-term instrumental drifts in water vapor and nitrous oxide measurements from the Aura Microwave Limb Sounder (MLS) and their implications for studies of variability and trends, Atmospheric Chemistry and Physics, 21, 15 409–15 430, https://doi.org/10.5194/acp-21-15409-2021, 2021.

Lu, H., Hitchman, M. H., Gray, L. J., Anstey, J. A., and Osprey, S. M.: On the role of Rossby wave breaking in the quasi-biennial modulation of the stratospheric polar vortex during boreal winter, Quarterly Journal of the Royal Meteorological Society, 146, 1939–1959, https://doi.org/https://doi.org/10.1002/qj.3775, 2020.

Manney, G. L., Millan, L. F., Santee, M. L., Wargan, K., Lambert, A., Neu, J. L., Werner, F., Lawrence, Z. D., Schwartz, M. J., Livesey, N. J., and Read, W. G.: Signatures of Anomalous Transport in the 2019/2020 Arctic Stratospheric Polar Vortex, Journal of Geophysical Research: Atmospheres, 127, e2022JD037 407, https://doi.org/https://doi.org/10.1029/2022JD037407, e2022JD037407 2022JD037407, 2022.

Ménard, R., Chabrillat, S., Robichaud, A., de Grandpré, J., Charron, M., Rochon, Y., Batchelor, R., Kallaur, A., Reszka, M., and Kaminski, J. W.: Coupled stratospheric chemistry–meteorology data assimilation. part i: Physical background and coupled modeling aspects, Atmosphere, 11, 150, 2020.

Minganti, D.: Supplement for: Datasets of QBO-induced anomalous transport in the Northern Hemisphere stratosphere: the exceptional 2018/2019 late boreal winter, https://doi.org/https://doi.org/10.18758/wfv3fdib, 2026.

Minganti, D., Chabrillat, S., Christophe, Y., Errera, Q., Abalos, M., Prignon, M., Kinnison, D. E., and Mahieu, E.: Climatological impact of the Brewer-Dobson circulation on the $N_2O$ budget in WACCM, a chemical reanalysis and a CTM driven by four dynamical reanalyses, Atmospheric Chemistry and Physics, 20, 12 609–12 631, https://doi.org/10.5194/acp-20-12609-2020, 2020.

https://doi.org/10.5194/egusphere-2026-3449
Preprint. Discussion started: 25 June 2026


Minganti, D., Chabrillat, S., Errera, Q., Prignon, M., Kinnison, D. E., Garcia, R. R., Abalos, M., Alsing, J., Schneider, M., Smale, D., et al.: Evaluation of the N2O Rate of Change to Understand the Stratospheric Brewer-Dobson Circulation in a Chemistry-Climate Model, Journal of Geophysical Research: Atmospheres, 127, e2021JD036 390, 2022.

Nevison, C. D., Liang, Q., Newman, P. A., Stephens, B. B., Dutton, G., Lan, X., Commane, R., Gonzalez, Y., and Kort, E.: Observational and model evidence for a prominent stratospheric influence on variability in tropospheric nitrous oxide, Atmospheric Chemistry and Physics, 24, 10 513–10 529, https://doi.org/10.5194/acp-24-10513-2024, 2024.

Nielsen, J. E., Pawson, S., Molod, A., Auer, B., Da Silva, A. M., Douglass, A. R., Duncan, B., Liang, Q., Manyin, M., Oman, L. D., et al.: Chemical mechanisms and their applications in the Goddard Earth Observing System (GEOS) earth system model, Journal of Advances in Modeling Earth Systems, 9, 3019–3044, 2017.

Orbe, C., Oman, L. D., Strahan, S. E., Waugh, D. W., Pawson, S., Takacs, L. L., and Molod, A. M.: Large-Scale Atmospheric Transport in GEOS Replay Simulations, Journal of Advances in Modeling Earth Systems, 9, 2545–2560, https://doi.org/https://doi.org/10.1002/2017MS001053, 2017.

Orbe, C., Plummer, D. A., Waugh, D. W., Yang, H., Jöckel, P., Kinnison, D. E., Josse, B., Marecal, V., Deushi, M., Abraham, N. L., et al.: Description and Evaluation of the specified-dynamics experiment in the Chemistry-Climate Model Initiative, Atmospheric Chemistry and Physics, 20, 3809–3840, 2020.

Park, J.-S., Park, S.-H., Chun, H.-Y., Yoo, J.-H., and Shin, U.: Analysis of planetary scale waves using Idealized sudden stratospheric warming simulations in different dynamical cores, Journal of Geophysical Research: Atmospheres, 129, e2023JD039 703, 2024.

Pascoe, C. L., Gray, L. J., Crooks, S. A., Juckes, M. N., and Baldwin, M. P.: The quasi-biennial oscillation: Analysis using ERA-40 data, Journal of Geophysical Research: Atmospheres, 110, https://doi.org/https://doi.org/10.1029/2004JD004941, 2005.

Petropavlovskikh, I., De Mazière, M., Thompson, A. M., Wild, J. D., Hannigan, J. W., Selkirk, H. B., Hannum, R. A., Steinbrecht, W., Lambert, J.-C., Van Malderen, R., Asher, E., Cordero, R. R., Godin-Beekmann, S., Hubert, D., Khaykin, S., Kreher, K., Leblanc, T., Mahieu, E., Maillard Barras, E., McConville, G., Nedoluha, G., Ortega, I., Redondas Marrero, A., Seckmeyer, G., Stauffer, R. M., Strode, S. A., Strong, K., Sugita, T., Van Roozendael, M., Velazco, V., Vigouroux, C., and Vogel, B.: The Network for the Detection of Atmospheric Composition Change at 35 Years: Achievements and Future Strategy, EGUsphere, 2026, 1–52, https://doi.org/10.5194/egusphere-2025-6557, 2026.

Ploeger, F., Legras, B., Charlesworth, E., Yan, X., Diallo, M., Konopka, P., Birner, T., Tao, M., Engel, A., and Riese, M.: How robust are stratospheric age of air trends from different reanalyses?, Atmospheric Chemistry and Physics, 19, 6085–6105, 2019.

Ploeger, F., Diallo, M., Charlesworth, E., Konopka, P., Legras, B., Laube, J. C., Grooß, J.-U., Günther, G., Engel, A., and Riese, M.: The stratospheric Brewer–Dobson circulation inferred from age of air in the ERA5 reanalysis, Atmospheric Chemistry and Physics, 21, 8393–8412, 2021.

Plumb, R. A.: Stratospheric transport, Journal of the Meteorological Society of Japan. Ser. II, 80, 793–809, 2002.

Plumb, R. A. and Bell, R. C.: A model of the quasi-biennial oscillation on an equatorial beta-plane, Quarterly Journal of the Royal Meteorological Society, 108, 335–352, 1982.

Prather, M. J., Hsu, J., DeLuca, N. M., Jackman, C. H., Oman, L. D., Douglass, A. R., Fleming, E. L., Strahan, S. E., Steenrod, S. D., Søvde, O. A., et al.: Measuring and modeling the lifetime of nitrous oxide including its variability, Journal of Geophysical Research: Atmospheres, 120, 5693–5705, 2015.

Prather, M. J., Froidevaux, L., and Livesey, N. J.: Observed changes in stratospheric circulation: decreasing lifetime of $N_2O$, 2005–2021, Atmospheric Chemistry and Physics, 23, 843–849, https://doi.org/10.5194/acp-23-843-2023, 2023.

https://doi.org/10.5194/egusphere-2026-3449
Preprint. Discussion started: 25 June 2026


Rosenlof, K. H.: Seasonal cycle of the residual mean meridional circulation in the stratosphere, Journal of Geophysical Research: Atmospheres, 100, 5173–5191, 1995.

Salawitch, R. J., Smith, J. B., Selkirk, H., Wargan, K., Chipperfield, M. P., Hossaini, R., Levelt, P. F., Livesey, N. J., McBride, L. A., Millan, L. F., Moyer, E., Santee, M. L., Schoeberl, M. R., Solomon, S., Stone, K., and Worden, H. M.: The Imminent Data Desert: The Future of Stratospheric Monitoring in a Rapidly Changing World, Bulletin of the American Meteorological Society, https://doi.org/10.1175/BAMS-D-23-0281.1, 2025.

Seinfeld, J. H. and Pandis, S. N.: Atmospheric chemistry and physics: from air pollution to climate change, John Wiley & Sons, 2016.

Shepherd, T. G.: Transport in the middle atmosphere, Journal of the Meteorological Society of Japan. Ser. II, 85, 165–191, 2007.

Smith, A. K., Garcia, R. R., Moss, A. C., and Mitchell, N. J.: The semiannual oscillation of the tropical zonal wind in the middle atmosphere derived from satellite geopotential height retrievals, Journal of the Atmospheric Sciences, 74, 2413–2425, 2017.

Smith, A. K., Gray, L. J., and Garcia, R. R.: Evidence for the influence of the quasi-biennial oscillation on the semiannual oscillation in the tropical middle atmosphere, Journal of the Atmospheric Sciences, 80, 1755–1769, 2023.

Steinbrecht, W., Köhler, U., Claude, H., Weber, M., Burrows, J., and Van Der A, R.: Very high ozone columns at northern mid-latitudes in 2010, Geophysical research letters, 38, 2011.

Stocker, M., Ladstädter, F., and Steiner, A. K.: Observing the climate impact of large wildfires on stratospheric temperature, Scientific reports, 11, 22 994, 2021.

Strahan, S., Oman, L., Douglass, A., and Coy, L.: Modulation of Antarctic vortex composition by the quasi-biennial oscillation, Geophysical Research Letters, 42, 4216–4223, 2015.

Strode, S. A., Ziemke, J. R., Oman, L. D., Lamsal, L. N., Olsen, M. A., and Liu, J.: Global changes in the diurnal cycle of surface ozone, Atmospheric Environment, 199, 323–333, 2019.

Tian, H., Xu, R., Canadell, J. G., Thompson, R. L., Winiwarter, W., Suntharalingam, P., Davidson, E. A., Ciais, P., Jackson, R. B., Janssens-Maenhout, G., Prather, M. J., Regnier, P., Pan, N., Pan, S., Peters, G. P., Shi, H., Tubiello, F. N., Zaehle, S., Zhou, F., Arneth, A., Battaglia, G., Berthet, S., Bopp, L., Bouwman, A. F., Buitenhuis, E. T., Chang, J., Chipperfield, M. P., Dangal, S. R. S., Dlugokencky, E., Elkins, J. W., Eyre, B. D., Fu, B., Hall, B., Ito, A., Joos, F., Krummel, P. B., Landolfi, A., Laruelle, G. G., Lauerwald, R., Li, W., Lienert, S., Maavara, T., MacLeod, M., Millet, D. B., Olin, S., Patra, P. K., Prinn, R. G., Raymond, P. A., Ruiz, D. J., van der Werf, G. R., Vuichard, N., Wang, J., Weiss, R. F., Wells, K. C., Wilson, C., Yang, J., and Yao, Y.: A comprehensive quantification of global nitrous oxide sources and sinks, Nature, 586, 248–256, https://doi.org/10.1038/s41586-020-2780-0, 2020.

Tuckett, R.: Greenhouse Gases, in: Encyclopedia of Analytical Science (Third Edition), edited by Worsfold, P., Poole, C., Townshend, A., and Miró, M., pp. 362–372, Academic Press, Oxford, third edition edn., ISBN 978-0-08-101984-9, https://doi.org/https://doi.org/10.1016/B978-0-12-409547-2.14031-4, 2019.

Vervalcke, S., Errera, Q., Eichinger, R., Reddmann, T., Chabrillat, S., Op de beeck, M., Stiller, G., and Mahieu, E.: Atmospheric lifetime of sulphur hexafluoride ($SF_6$) and five other trace gases in the BASCOE model driven by three reanalyses, Atmospheric Chemistry and Physics, 26, 391–409, https://doi.org/10.5194/acp-26-391-2026, 2026.

Wargan, K., Kramarova, N., Weir, B., Pawson, S., and Davis, S. M.: Toward a Reanalysis of Stratospheric Ozone for Trend Studies: Assimilation of the Aura Microwave Limb Sounder and Ozone Mapping and Profiler Suite Limb Profiler Data, Journal of Geophysical Research: Atmospheres, 125, e2019JD031 892, https://doi.org/https://doi.org/10.1029/2019JD031892, e2019JD031892 2019JD031892, 2020a.

https://doi.org/10.5194/egusphere-2026-3449
Preprint. Discussion started: 25 June 2026


Wargan, K., Weir, B., Manney, G. L., Cohn, S. E., and Livesey, N. J.: The Anomalous 2019 Antarctic Ozone Hole in the GEOS Constituent Data Assimilation System With MLS Observations, Journal of Geophysical Research: Atmospheres, 125, e2020JD033 335, https://doi.org/https://doi.org/10.1029/2020JD033335, e2020JD033335 2020JD033335, 2020b.

Wargan, K., Weir, B., Manney, G. L., Cohn, S. E., Knowland, K. E., Wales, P. A., and Livesey, N. J.: M2-SCREAM: A stratospheric composition reanalysis of Aura MLS data with MERRA-2 transport, Earth and Space Science, 10, e2022EA002 632, 2023.

Waters, J. W., Froidevaux, L., Harwood, R. S., Jarnot, R. F., Pickett, H. M., Read, W. G., Siegel, P. H., Cofield, R. E., Filipiak, M. J., Flower, D. A., et al.: The earth observing system microwave limb sounder (EOS MLS) on the Aura satellite, IEEE Transactions on Geoscience and Remote Sensing, 44, 1075–1092, 2006.

Weir, B., Crisp, D., OŽ019Dell, C. W., Basu, S., Chatterjee, A., Kolassa, J., Oda, T., Pawson, S., Poulter, B., Zhang, Z., et al.: Regional impacts of COVID-19 on carbon dioxide detected worldwide from space, Science advances, 7, eabf9415, 2021.

Weir, B., Wargan, K., Keller, C. A., Knowland, K. E., Wales, P. A., Shah, V., Karpowicz, B. M., Balashov, N., Ott, L. E., Todling, R., et al.: Atmospheric Constituent Data Assimilation in NASA's Goddard Earth Observing System, Authorea Preprints, 2026.

Wilmouth, D. M., Østerstrøm, F. F., Smith, J. B., Anderson, J. G., and Salawitch, R. J.: Impact of the Hunga Tonga volcanic eruption on stratospheric composition, Proceedings of the National Academy of Sciences, 120, e2301994 120, https://doi.org/10.1073/pnas.2301994120, 2023.

WMO: Scientific assessment of ozone depletion: 2022. Global Ozone Research and Monitoring Project–Report No. 278, Geneva, Switzerland, 2022.

Yamazaki, K., Nakamura, T., Ukita, J., and Hoshi, K.: A tropospheric pathway of the stratospheric quasi-biennial oscillation (QBO) impact on the boreal winter polar vortex, Atmospheric Chemistry and Physics, 20, 5111–5127, 2020.

Yu, P., Davis, S. M., Toon, O. B., Portmann, R. W., Bardeen, C. G., Barnes, J. E., Telg, H., Maloney, C., and Rosenlof, K. H.: Persistent stratospheric warming due to 2019–2020 Australian wildfire smoke, Geophysical Research Letters, 48, e2021GL092 609, 2021.

Yu, W., Garcia, R., Yue, J., Russell III, J., and Mlynczak, M.: Variability of Water Vapor in the Tropical Middle Atmosphere Observed From Satellites and Interpreted Using SD-WACCM Simulations, Journal of Geophysical Research: Atmospheres, 127, e2022JD036 714, https://doi.org/https://doi.org/10.1029/2022JD036714, e2022JD036714 2022JD036714, 2022.